Circular Dichroism and Magnetic Circular Dichroism Studies of the Fully Reduced Binuclear Non-Heme Iron Active Site in the *Escherichia coli* R2 Subunit of Ribonucleoside Diphosphate Reductase

Sabine Coates Pulver,[†] Wing H. Tong,[‡] J. Martin Bollinger,[‡] Joanne Stubbe,*[,‡] and Edward I. Solomon*[,†]

Contribution from the Department of Chemistry, Stanford University, Stanford, California 94305, and Department of Chemistry, Massachusetts Institute of Technology, Cambridge, Massachusetts 02139

Received August 23, 1995[⊗]

Abstract: A combination of circular dichroism (CD) and magnetic circular dichroism (MCD) spectroscopies has been used to probe the geometric and electronic structure of the binuclear Fe(II) active site of the R2 subunit of reduced ribonucleoside diphosphate reductase (R2 RDPR). Excited state data provide the numbers and energies of d → d transitions which are used to estimate the geometry of each iron atom. Variable-temperature variable-field (VTVH) MCD data are analyzed by using a non-Kramers doublet model to obtain the zero-field splitting (ZFS) and $g_{\|}$ value of the ground state and the excited state sublevel energies. These results are further interpreted in terms of a spin Hamiltonian which includes the ZFS of each Fe(II) atom combined with the exchange coupling, J, between iron centers. The fully reduced R2 active site is best described as one five- and one four-coordinate Fe(II) atom. The ferrous atoms are weakly antiferromagnetically coupled, $J \approx -0.5$ cm^{-1}, and have opposite ZFS values consistent with iron atoms in different coordination environments. Azide binding studies indicate that reduced R2 has two binding constants for azide which were determined to be 21 ± 4 M^{-1} and 3 ± 1 M^{-1}. The active site of the one-azide-bound R2 complex consists of one four- and one six-coordinate Fe(II) atom. VTVH MCD data show the ferrous centers to be antiferromagnetically coupled, $J \approx -2.5$ cm^{-1}. These results suggest that azide binding alters both the geometric and electronic structure of the reduced R2 ground state. High excess azide further perturbs the binuclear ferrous active site and leads to the formation of two distinct two-azide-bound R2 complexes. One component is ferromagnetically coupled, $J \approx 1.0$ cm^{-1}, and is associated with a five- and six-coordinate biferrous center. The second component is weakly coupled, $-2.0 < J < 2.0$ cm^{-1}, and consists of one four- and one six-coordinate Fe(II) atom. The azide binding studies are compared to parallel results for deoxyhemerythrin (deoxyHr) and the hydroxylase component of methane monooxygenase (MMOH), and differences are correlated to differences in the bridging ligation of the binuclear ferrous active site.

Introduction

Binuclear non-heme iron centers have been identified as the catalytic active sites in a large number of proteins and enzymes whose mechanisms involve interactions of dioxygen with a ferrous site.[1] This class of proteins includes hemerythrin (Hr, oxygen transport and storage),[2,3] ribonucleoside diphosphate reductase (RDPR, formation of a catalytically active tyrosine radical),[4−6] methane monooxygenase (MMO, activation of dioxygen for insertion into carbon−hydrogen bonds),[7−9] the purple acid phosphatases (PAP, inactivated by dioxygen in the presence of phosphate),[10−13] acyl carrier protein Δ^9 desaturase (ACP Δ^9D, activation of dioxygen for the insertion of a 9,10 *cis* double bond),[14,15] and rubrerythrin (Rb, unknown).[16,17] The binuclear iron site can occur in any of three oxidation states: met [Fe(III)Fe(III)], half-met (or mixed valent) [Fe(III)Fe(II)], and deoxy (or fully reduced) [Fe(II)Fe(II)]. All three oxidation states have been observed in Hr, RDPR and MMO.[1]

Ribonucleoside diphosphate reductase catalyzes the reduction of nucleotides to 2′-deoxynucleotides, the first committed and rate limiting step of DNA biosynthesis.[4,6,18] RDPR from *Escherichia coli* is a two component enzyme consisting of a 172-kDa homodimeric protein denoted R1 with an α_2 subunit

[†] Stanford University.
[‡] Massachusetts Institute of Technology.
[⊗] Abstract published in *Advance ACS Abstracts*, December 1, 1995.

(1) Feig, A. L.; Lippard, S. J. *Chem. Rev.* **1994**, *94*, 759.
(2) Wilkins, P. C.; Wilkins, R. G. *Coord. Chem. Rev.* **1987**, *79*, 195.
(3) Klotz, I. M.; Kurtz, D. M. *Acc. Chem. Res.* **1984**, *17*, 16.
(4) Stubbe, J. *J. Biol. Chem.* **1990**, *265*, 5329.
(5) Nordlund, P.; Eklund, H. *J. Mol. Biol.* **1993**, *232*, 123.
(6) Reichard, P.; Ehrenberg, A. *Science* **1983**, *221*, 514.
(7) Lipscomb, J. D. *Annu. Rev. Microbiol.* **1994**, *48*, 371.
(8) Fox, B. G.; Lipscomb, J. D. In *Biological Oxidation Systems*; Reddy, C. C., Hamilton, G. A., Madyastha, K. M., Eds.; Academic Press: New York, 1992; Vol. 1, p 367.
(9) Dalton, H. In *Advances in Applied Microbiology*; Umbreit, W. W., Ed.; Academic Press: New York, 1980; Vol. 26, p 71.
(10) Doi, K.; Antanaitis, C.; Aisen, P. In *Structure and Bonding*; Clarke, M. J., Goodenough, J. B., Ibers, J. A., Jorgensen, C. K., Mingos, D. M. P., Neilands, J. B., Palmer, G. A., Reinen, D., Sadler, P. J., Weiss, R., and Williams, R. J. P., Eds.; Springer-Verlag: Heidelberg, 1988; Vol. 70, p 1.
(11) Antanaitis, B. C.; Aisen, P. In *Frontiers in Bioinorganic Chemistry*; Xavier, A. V., Ed.; VCH: New York, 1986; p 481.
(12) Que, L.; Scarrow, R. C. In *Metal Clusters in Proteins*; Que, L., Ed.; American Chemical Society: Washington, DC, 1988; p 152.
(13) Vincent, J. B.; Averill, B. A. *FASEB J.* **1990**, *4*, 3009.
(14) Nagai, J.; Bloch, K. *J. Biol. Chem.* **1968**, *243*, 4626.
(15) Fox, B. G.; Shanklin, J.; Somerville, C.; Münck, E. *Proc. Natl. Acad. Sci. U.S.A.* **1993**, *90*, 2486.
(16) LeGall, B. G.; Prickril, B. C.; Moura, I.; Xavier, A. V. *Biochemistry* **1988**, *27*, 1636.
(17) Gupta, N.; Bonomi, F.; Kurtz, D. M.; Ravi, N.; Wang, D. L.; Huynh, B. H. *Biochemistry* **1995**, *34*, 3310.
(18) Sjöberg, B.-M.; Gräslund, A. In *Advances in Inorganic Biochemistry*; Theil, E. C., Eichorn, G. L., and Marzilli, L. G., Ed.; Elsevier: 1983; Vol. 5, p 87.

0002-7863/95/1517-12664$09.00/0

structure and an 87-kDa dimeric protein called R2 having a β_2 subunit structure.[5,19] The R1 subunit contains the binding sites for the substrate and allosteric effectors and also contains multiple cysteine residues which cycle between sulfhydryl and disulfide forms to deliver reducing equivalents to the substrate.[4,20-23] The smaller R2 subunit contains one to two non-heme iron clusters each containing a coupled binuclear iron active site and a stable tyrosyl radical at residue 122.[5,19] The tyrosyl radical is essential and is thought to participate in the enzymatic reaction by creating a thiyl radical on the R1 subunit which generates a reactive substrate radical to initiate nucleotide reduction.[4] Mössbauer studies and iron assays have shown that the binuclear iron site is responsible for the formation of the tyrosyl radical and that the assembly of the R2 cofactor can occur spontaneously.[24]

Mössbauer studies on the oxidized R2 subunit[24-26] demonstrated that the diferric center is diamagnetic at low temperature due to antiferromagnetic coupling between the two Fe(III) atoms. Extended X-ray absorption fine structure (EXAFS) studies give an Fe···Fe distance of 3.4 Å and provide evidence for a short μ-oxo bridge.[27,28] Resonance Raman[29] and UV−vis absorbance[25] also point to the presence of a μ-oxo bridge. Magnetic susceptibility studies showed that the exchange coupling, J, was on the order of -108 cm^{-1} ($H = -2JS_1 \cdot S_2$),[25] which is consistent with a Fe(III)−O−Fe(III) moiety. The presence of the oxo bridge is also supported by the crystal structure of the met form of the R2 subunit of RDPR.[5,19]

The three-dimensional structure of met-R2 has been determined by X-ray crystallography at 2.2 Å resolution.[5,19] The two β protomers are related by a molecular 2-fold rotation axis and are linked to produce a heart-shaped molecule. Each protomer contains a binuclear iron cluster, and the iron centers are separated by a distance of 25 Å. Within each binuclear cluster, the Fe(III)···Fe(III) distance is 3.3 Å, and the iron atoms are bridged by one carboxylate ligand derived from the protein (Glu 115) and a μ-oxo bridge, which has been shown to originate from O_2.[30] In addition to the bridging ligands, one Fe(III) ion is coordinated to one histidine (His 241), two monodentate carboxylate residues (Glu 238 and 204), and a water molecule. The coordination sphere of the other Fe(III) ion is completed by one histidine residue (His 118), one bidentate carboxylate residue (Asp 84), and a terminal water ligand.

Electronic absorption and electron paramagnetic resonance (EPR) studies have shown that the binuclear ferrous form of the R2 subunit reacts with dioxygen to generate the tyrosine radical.[25] There have been a limited number of spectroscopic studies aimed at defining the geometric and electronic structure of the ferrous site of R2. Nuclear magnetic resonance (NMR) studies[31] and magnetic susceptibility measurements[32] show that the ferrous active site is weakly coupled. Mössbauer[26] and circular dichroism[33] (CD) studies predicted that the two Fe(II) atoms are in different coordination environments. EPR studies[34] revealed that small molecules interact with the biferrous active site. It should be noted that preliminary crystallographic data on the reduced iron active site are available.[35] The Fe(II) atoms are bridged by two protein-derived glutamic acid residues (Glu 238 and 115), and the coordination environment of one Fe(II) atom is completed by a histidine (His 118) and an aspartic acid residue (Asp 84) and the other Fe(II) atom by a histidine (His 241) and a glutamic acid residue (Glu 204), resulting in two essentially equivalent four-coordinate Fe(II) centers. However, the coordination environment of reduced RDPR observed by X-ray crystallography differs from expectations based on the Mössbauer[26] and CD[33] results.

At present the ligand environment of the fully reduced [Fe(II)Fe(II)] R2 subunit of RDPR is not fully understood. Circular dichroism and magnetic circular dichroism (MCD) spectroscopies provide direct probes of non-heme ferrous active sites, since they allow the observation of ferrous ligand field (d → d) transitions which are often weak in absorption, and the temperature and field dependence of the MCD is sensitive to ground state splittings. CD and MCD have been very effective techniques in elucidating the geometric and electronic structure of the binuclear ferrous active site of deoxyHr[36] and of the reduced hydroxylase component of MMO (MMOH).[37] These studies have shown that the reduced MMOH site contains two five-coordinate Fe(II) atoms with different geometries. Variable-temperature variable-field (VTVH) MCD studies demonstrated that the ground state has a $g_{eff} = 14.7$ which required that the two ferrous ions be weakly ferromagnetically coupled ($J \approx 0.3$ cm^{-1}) with each undergoing zero-field splitting to produce an $S_{Tot} = 4$, $M_s = \pm 4$ ground state. Parallel studies on deoxyHr have shown that the deoxyHr site consists of one five- and one six-coordinate Fe(II) atom that are antiferromagnetically coupled through a bridging hydroxide ligand.[36] The results of these studies are supported by X-ray crystallography[38,39] and provide additonal insight into the electronic structure of the reduced site and its interactions with exogenous ligands which are related to mechanism. In order to understand the active site structure of fully reduced R2, we have extended our earlier near-IR CD studies to include VTVH MCD data, ground state analyses, and the effects of small molecule interactions on the CD and MCD data. Small molecule binding interactions can reflect O_2 interaction with the site and define differences among coupled binuclear non-heme iron proteins.

A combination of excited state spectral methods (CD and low-temperature MCD) are used to study the ligand field region from 5000 to 18000 cm^{-1}, and VTVH MCD is used to probe

(19) Nordlund, P.; Sjöberg, B.-M.; Eklund, H. *Nature* **1990**, *45*, 593.
(20) von Döbeln, U.; Reichard, P. *J. Biol. Chem.* **1976**, *251*, 3616.
(21) Brown, N. C.; Reichard, P. *J. Biol. Chem.* **1969**, *46*, 39.
(22) Thelander, L. *J. Biol. Chem.* **1974**, *249*, 4858.
(23) Uhlin, U.; Eklund, H. *Nature* **1994**, *370*, 533.
(24) Atkin, C. L.; Thelander, L.; Reichard, P.; Lang, G. *J. Biol. Chem.* **1973**, *248*, 7464.
(25) Petersson, L.; Gräslund, A.; Ehrenberg, A.; Sjöberg, B.-M.; Reichard, P. *J. Biol. Chem.* **1980**, *255*, 6706.
(26) Lynch, J. B.; Juarez-Garcia, C.; Münck, E.; Que, L. *J. Biol. Chem.* **1989**, *264*, 8091.
(27) Scarrow, R. C.; Maroney, M. J.; Palmer, S. M.; Que, L.; Roe, A. L.; Salowe, S. P.; Stubbe, J. *J. Am. Chem. Soc.* **1987**, *109*, 7857.
(28) Bunker, G.; Peterson, L.; Sjöberg, B.-M.; Sahlin, M.; Chance, M.; Chance, B.; Ehrenberg, A. *Biochemistry* **1987**, *26*, 4708.
(29) Sjöberg, B.-M.; Loehr, T. M.; Sanders-Loehr, J. *Biochemistry* **1982**, *21*, 96.
(30) Ling, J.; Sahlin, M.; Sjöberg, B.-M.; Loehr, T. M.; Sanders-Loehr, J. *J. Biol. Chem.* **1994**, *269*, 5595.
(31) Sahlin, M.; Gräslund, A.; Petersson, L.; Ehrenberg, A.; Sjöberg, B.-M. *Biochemistry* **1989**, *28*, 2618.
(32) Atta, M.; Scheer, C.; Fries, P. H.; Fontecave, M.; Latour, J.-M. *Angew. Chem., Int. Ed. Engl.* **1992**, *31*, 1513.
(33) McCormick, J. M.; Reem, R. C.; Foroughi, J.; Bollinger, J. M.; Jensen, G. M.; Stephens, P. J.; Stubbe, J.; Solomon, E. I. *New J. Chem.* **1991**, *6*, 439.
(34) Elgren, T. E.; Hendrich, M. P.; Que, L., Jr. *J. Am. Chem. Soc.* **1993**, *115*, 9291.
(35) (a) Nordlund, P.; Eklund, H.; Åberg, A.; deMare, X.-D. *Abstracts of Papers*, 209th National Meeting of the American Chemical Society, Anaheim, CA, 1995; American Chemical Society: Washington, DC, 1995; Abstract 209. (b) Personal communication.
(36) Reem, R. C.; Solomon, E. I. *J. Am. Chem. Soc.* **1987**, *109*, 1216.
(37) Pulver, S.; Froland, W. A.; Fox, B. G.; Lipscomb, J. D.; Solomon, E. I. *J. Am. Chem. Soc.* **1993**, *115*, 12409.
(38) Holmes, M. A.; Trong, I. L.; Turley, S.; Sieker, L. C.; Stenkamp, R. E. *J. Mol. Biol.* **1991**, *218*, 583.
(39) Rosenzweig, A. C.; Nordlund, P.; Takahara, P. M.; Frederick, C. A.; Lippard, S. J. *Chem. Biol.* **1995**, *2*, 409.

the ground state sublevels of fully reduced R2. In addition, the interaction of the fully reduced R2 active site with small molecules has been investigated. This study allows the definition of differences and similarities in the electronic and geometric structure of deoxyHr, reduced MMOH, and reduced R2, the results of which are related to differences in the reactivity of these proteins with molecular oxygen.

Material and Methods

All commercial reagents were used as obtained: HEPES buffer (Sigma, Mallinckrodt), sodium chloride (Sigma), sodium azide (Aldrich), hydroxylamine sulfate (Eastman), methyl viologen (Sigma), sodium dithionite (Fisher), D_2O (99.9 atom % D; Aldrich), d_3-glycerol (98 atom %; Aldrich, Cambridge Isotope Laboratories).

The R2 subunit of ribonucleoside diphosphate reductase was isolated from the heat-inducible overproducing strain (N6405/pSPS2) of *E. coli* as described previously.[40] The specific activity for the R2 subunit was 6000–7000 nmol/min/mg (~3.3 mol Fe/mol R2). Met-R2 was prepared by incubating native R2 with hydroxylamine sulfate (final concentration 25 mM) for 30 min at room temperature in order to reduce the tyrosyl radical. Next, the protein was transferred to a 12000–14000 molecular weight cutoff dialysis bag. Fully reduced R2 samples were prepared by anaerobic dialysis of met-R2 against ~5 mM sodium dithionite and ~20 μM methyl viologen in 400 mM HEPES buffer, pD 7.6 at 4 °C for 10–20 h. The fully reduced R2 concentration was determined by conversion to native R2 (ϵ_{280} = 130.5 mM^{-1} cm^{-1}) through exposure to air.

The effects of small molecule binding were investigated by the anaerobic addition of microliter quantities of a thoroughly degassed ligand solution to the fully reduced R2 subunit of RDPR in a CD cell. The concentration of small molecules added to the protein sample was varied, up to a 2000-fold molar excess. All samples were incubated for approximately 15 min before spectra were recorded. All ligand solutions were prepared in D_2O and deoxygenated with two–three freeze–pump–thaw cycles at 10^{-3} Torr unless otherwise noted. Since reduced R2 readily oxidizes, extreme care was taken to ensure anaerobic conditions. The CD cuvette was sealed with a rubber septum and evacuated and back-filled with argon on a Schlenk line five–ten times prior to use. Argon was deoxygenated by passing the gas over a hydrogen-reduced copper-based catalyst. Spectra were recorded under a constant nitrogen purge over the CD cell. For the azide titration experiments, 200 μL was drawn into a gas-tight 250 μL Hamilton syringe equipped with a 25-gauge needle. After a one-time insertion of the syringe into the stoppered CD cuvette, 5 μL additions of azide were made.

Near-IR CD spectra (600–2000 nm) were obtained on a Jasco 200D spectropolarimeter with an InSb detector. Samples were placed in a 2 mm pathlength near-infrared quartz cuvette and cooled to 5 °C by a recirculating water bath. Low-temperature CD and MCD spectroscopic experiments were performed using the Jasco spectropolarimeter, equipped with a modified sample compartment to accommodate focusing optics[41] and an Oxford Instruments Spectromag 4 superconducting (Oxford SM4-7T) magnet/cryostat.

CD samples (~0.8–1.4 mM) of the fully reduced R2 were prepared by anaerobically withdrawing a ~100 μL aliquot of reduced protein from the dialysis set-up and injecting the sample into a cuvette previously sealed with a septum and deoxygenated.

Protein samples (~0.4–1.0 mM) for MCD experiments were prepared as anaerobic glasses in 66% (v/v) d_3-glycerol/0.4 M HEPES buffer, pD 7.6. Samples were injected anaerobically into an argon-purged MCD cell made by compressing a 2–3 mm rubber spacer between two quartz discs. Depolarization of the light by the MCD glass samples was monitored by their effect on the CD signal of a nickel (+)-tartrate solution placed before and after the sample.[42] In all cases, the depolarization was <10% at 4.2 K.

(40) Salowe, S.; Stubbe, J. *J. Bacteriol.* **1986**, *165*, 363.
(41) Spira-Solomon, D. J.; Allendorf, M. D.; Solomon, E. I. *J. Am. Chem. Soc.* **1986**, *108*, 5318.
(42) Browett, W. R.; Fucaloro, A. F.; Morgan, T. V.; Stephens, P. J. *J. Am. Chem. Soc.* **1983**, *105*, 1868.

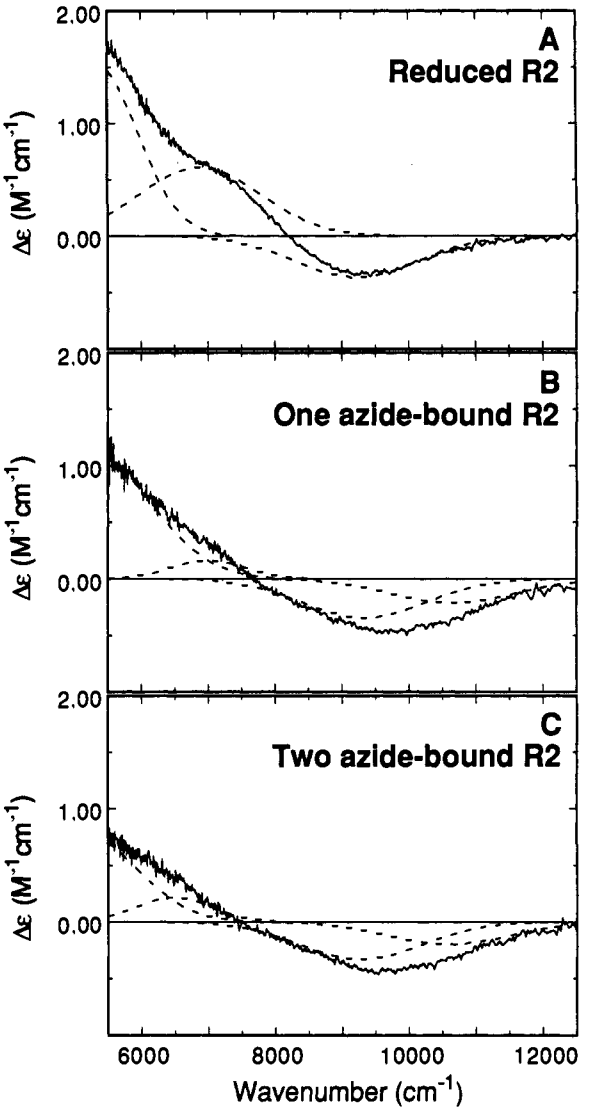

Figure 1. CD spectra of the binuclear non-heme Fe(II) active site in the R2 subunit of RDPR: (A) reduced R2; (B) the one-azide-bound R2 complex minus 34% reduced R2, renormalized; (C) the two-azide-bound R2 complex. The experimental data (—) were fit to individual Gaussian band shapes (- - -). CD spectra were recorded at 5 °C.

CD and MCD spectra were fit to Gaussian band shapes using a constrained nonlinear least-squares fitting procedure. Since each spectroscopic method has different selection rules, transitions can have different intensities and different signs. While the energies and bandwidths should be the same, the MCD spectra are taken at low temperature and thus may have significantly sharper bandwidths, and the band energies may shift slightly relative to the room temperature CD spectra, which was allowed for in the final fit.

Results

A. CD Data. Figure 1A presents the room temperature near-IR CD spectra of the fully reduced R2 subunit of RDPR from 5500 (the D_2O cutoff) to 12500 cm^{-1}. The CD spectrum of reduced R2 shows two overlapping positive bands in the region from 5000 to 7500 cm^{-1} and a negative feature at 9000 cm^{-1}. Control experiments show that these features are intrinsic to the Fe(II) active site: (1) quantitatively equivalent signals were obtained upon addition of 4 equiv of Fe(II) to apo R2; (2) addition of 2 equiv of Fe(II) to met-R2 did not produce these features; (3) addition of glycerol to the reduced R2 sample and cooling to 4.2 K produced no significant change in the CD spectrum. Gaussian spectral resolution can fit the spectrum to

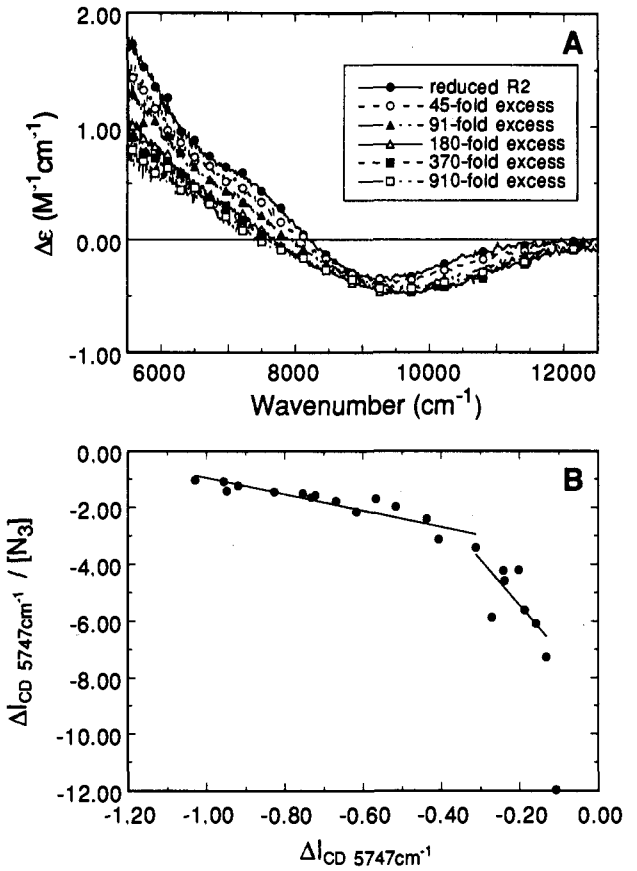

Figure 2. (A) CD spectra at 5 °C of reduced R2 in the presence of a 0- (●), 45- (○), 90- (▲), 180- (△), 370- (■), and 910-fold (□) molar excess of azide. (B) Scatchard plot showing the change in CD intensity at 5747 cm^{-1} plotted against the ratio of the $\Delta I_{CD\ 5747cm^{-1}}/[N_3^-]$.

three transitions at 5450 ± 150 cm^{-1} ($\Delta\epsilon$ = 1.5 ± 0.15 M^{-1} cm^{-1}), 7030 ± 100 cm^{-1} ($\Delta\epsilon$ = 0.6 ± 0.05 M^{-1} cm^{-1}), and9310 ± 150 cm^{-1} ($\Delta\epsilon$ = −0.32 ± 0.04 M^{-1} cm^{-1}). The dashed lines in Figure 1 show the full Gaussian-resolved CD spectra.

The CD spectrum of fully reduced R2 remains unchanged upon anaerobic addition of Cl^- and F^- at concentrations up to a 900-fold molar excess relative to protein (~1.5 mM R2). In contrast, addition of N_3^- and SCN^- induced a rapid change in the CD spectrum of reduced R2. Figure 2A presents the CD spectra of fully reduced R2 in the presence of a 45-, 90-, 200-, 400-, and 900-fold molar excess of azide. Further addition of azide produces no additional changes, indicating that the azide binding is saturated. Figure 2B shows the Scatchard plot[43] associated with the titration of fully reduced R2 with N_3^-. The change in CD intensity at 5747 cm^{-1} ($\Delta I_{CD\text{-}5747cm^{-1}}$) was measured over the course of the titration and is plotted against $\Delta I_{CD\text{-}5747cm^{-1}}$ divided by the azide concentration. The curvature in the titration data clearly indicates the presence of two binding constants for azide which were determined to be 21 ± 4 M^{-1} and 3 ± 1 M^{-1} for the first (low excess of N_3^-) and second (high excess of N_3^-) binding, respectively (Scheme 1). Exposure of the fully reduced ligand-bound forms to air generates the near-IR CD features characteristic of the tyrosyl radical associated with the native RDPR site, with a magnitude equivalent to that obtained by reacting reduced R2 with O_2 in the absence of exogenous ligands. This indicates that the presence of small molecules does not eliminate the O_2 reactivity of the site.

The one-azide-bound complex was studied by adding a ~90-fold molar excess of N_3^- to reduced R2 (1.1 mM). On the basis of the 21 M^{-1} value of the first binding constant, approximately 34% of the binuclear ferrous sites remained unreactive toward azide under these conditions and essentially no sites had been converted to the two-azide-bound species. Figure 1B presents the CD spectrum of the one-azide-bound complex. The contribution of the 34% unconverted reduced R2 sites to the CD spectrum was subtracted, and the spectrum was renormalized. The CD spectrum shows two low energy positive bands in the region from 5000 to 7500 cm^{-1} and a broad negative feature at ~9500 cm^{-1}. Gaussian spectral resolution indicates four transitions at 5200 ± 300 cm^{-1} ($\Delta\epsilon$ = 1.36 ± 0.2 M^{-1} cm^{-1}), 7215 ± 200 ($\Delta\epsilon$ = 0.22 ± 0.05 M^{-1} cm^{-1}), 9010 ± 200 ($\Delta\epsilon$ = −0.34 ± 0.05 M^{-1} cm^{-1}), and 10480 ± 100 ($\Delta\epsilon$ = −0.29 ± 0.05 M^{-1} cm^{-1}).

On the basis of the binding constants, only the two-azide-bound species is present when a 900-fold molar excess of N_3^- is added to reduced R2 (1.1 mM). The CD spectrum of this two-azide-bound complex is presented in Figure 1C. Gaussian spectral resolution indicates four transitions at 5300 ± 300 cm^{-1} ($\Delta\epsilon$ = 0.72 ± 0.03 M^{-1} cm^{-1}), 7220 ± 200 ($\Delta\epsilon$ = 0.15 ± 0.06 M^{-1} cm^{-1}), 9050 ± 150 ($\Delta\epsilon$ = −0.33 ± 0.05 M^{-1} cm^{-1}), and 10220 ± 100 ($\Delta\epsilon$ = −0.31 ± 0.03 M^{-1} cm^{-1}). The energies and band shapes of the transitions in the azide-bound complexes are unaffected by the glassing agent glycerol. Comparison between Figure 1, parts A, B and C reveals that the one-azide-bound complex and the two-azide-bound complex have three bands at approximately the same energy as fully reduced R2 and one additional high-energy feature. Ligand field peaks for reduced R2 and the one-azide-bound and two-azide-bound complexes are summarized in Table 1.

B. MCD Data. Figure 3A presents the low-temperature MCD spectrum of fully reduced R2. The MCD spectrum (5500−12000 cm^{-1}) shows two positive transitions at ~7500 cm^{-1} and <5500 cm^{-1}. Gaussian spectral resolution can fit the MCD spectrum to transitions at 5200 ± 200 ($\Delta\epsilon$ = 1.0 ± 0.5 M^{-1} cm^{-1}) and 7600 ± 200 cm^{-1} ($\Delta\epsilon$ = 4.0 ± 0.5 M^{-1} cm^{-1}). As the low-energy band extends beyond the low-energy limits of our detection, its energy and intensity are estimated from a Gaussian fit. The dashed lines in Figure 3 show the full Gaussian-resolved MCD spectra.

The low-temperature MCD spectrum of the one-azide-bound complex (Figure 3B) shows two positive bands centered at 5200 ($\Delta\epsilon$ = 3.0 ± 1.0 M^{-1} cm^{-1}) and 7570 cm^{-1} ($\Delta\epsilon$ = 4.7 ± 0.5 M^{-1} cm^{-1}), respectively. The contribution of 34% reduced R2 was subtracted from the MCD spectrum of the one-azide-bound complex and the data renormalized. Thus the low-energy CD bands of the one-azide-bound complex (Figure 1B) have corresponding transitions in MCD, while the high-energy features remain unobserved in MCD. Comparison of Figure 3, parts A and B reveals that the one-azide-bound complex has bands at approximately the same energy as fully reduced R2, but the band intensity of the low-energy band has increased upon azide binding. The ligand field bands observed in MCD are summarized in Table 1.

Figure 3C shows the low-temperature MCD spectrum of the two-azide-bound complex. The spectrum displays a number of bands, which can be Gaussian-resolved into two positive and one negative d → d transitions at 5300 ± 300 ($\Delta\epsilon$ = 3.0 ± 1.0 M^{-1} cm^{-1}), 7590 ± 200 ($\Delta\epsilon$ = 3.4 ± 0.5 M^{-1} cm^{-1}), and 10110 ± 100 ($\Delta\epsilon$ = −1.2 ± 0.02 M^{-1} cm^{-1}). Therefore, the two low-energy CD bands of the two-azide-bound complex (Figure 1C) are also observed in the MCD as is one of the negative higher-energy CD transitions. Comparison of the MCD spectra of the one-azide-bound and two-azide-bound complexes (Figure 3, parts B and C, respectively) shows that the two-azide-bound

(43) Connors, K. A. *Binding Constants*; John Wiley & Sons: New York, 1987.

Scheme 1

$$[Fe(II)Fe(II)] \underset{K_{low} \sim 21\ M^{-1}}{\overset{excess}{\rightleftharpoons}} [Fe(II)Fe(II)]\text{–}N_3^{\cdot} \underset{K_{high} \sim 3\ M^{-1}}{\overset{excess}{\rightleftharpoons}} [Fe(II)Fe(II)]\text{–}(N_3^{\cdot})_2$$

Table 1. Summary of CD and MCD Gaussian Fitting Results for Reduced R2, the One-Azide-Bound R2 Complex, and the Two-Azide-Bound R2 Complex

	reduced R2		one-azide-bound R2		two-azide-bound R2	
	energy (cm^{-1})	HWHM[a] (cm^{-1})	energy (cm^{-1})	HWHM (cm^{-1})	energy (cm^{-1})	HWHM (cm^{-1})
CD transitions						
band 1	5450 ± 150	1000 ± 100	5200 ± 300	1100 ± 200	5300 ± 300	1200 ± 100
band 2	7030 ± 100	1160 ± 100	7215 ± 200	1050 ± 200	7220 ± 200	1200 ± 200
band 3	9310 ± 150	1400 ± 100	9010 ± 200	1200 ± 100	9050 ± 150	1200 ± 100
band 4	–	–	10480 ± 100	1200 ± 100	10220 ± 200	1200 ± 200
MCD transitions						
band 1	5200 ± 300	1000 ± 200	5200 ± 300	1100 ± 200	5300 ± 300	1000 ± 200
band 2	7600 ± 200	1050 ± 100	7570 ± 200	1050 ± 100	7590 ± 200	1100 ± 100
band 3–	–	–	–	–	10110 ± 100	1100 ± 100

[a] HWHM = half-width at half-maximum height.

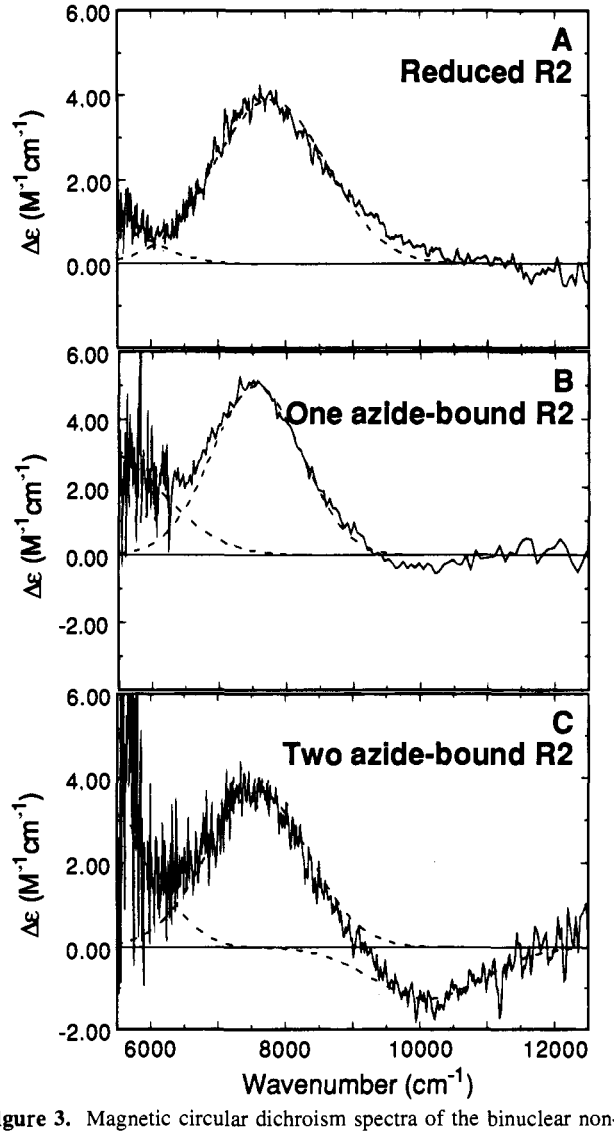

Figure 3. Magnetic circular dichroism spectra of the binuclear non-heme Fe(II) active site in the R2 subunit of RDPR: (A) reduced R2; (B) the one-azide-bound R2 complex minus 34% reduced R2, renormalized; (C) the two-azide-bound R2 complex. The experimental data (—) were fit to individual Gaussian band shapes (- - -). MCD spectra were recorded at 7.0 T and 4.2 K.

complex has two bands at approximately the same energy as the one-azide-bound complex and one additional negative feature at 10110 ± 100 cm^{-1}. Further addition of azide produces no additional change, indicating that the azide binding is saturated.

C. Saturation–Magnetization. The MCD transitions for reduced R2 and the R2–azide complexes increase in signal intensity as temperature decreases indicating that these transitions are MCD *C* terms. Thus the ground state of the fully reduced R2 and the azide-bound complexes are paramagnetic doublets which split in energy in a magnetic field. The field saturation curves measured on the positive band at 7700 cm^{-1} for reduced R2, the one-azide-bound complex, and the two azide-bound complex are shown in Figure 4 (parts A, B and C, respectively). The saturation–magnetization curve associated with the negative band at 10400 cm^{-1} in the two-azide-bound complex is shown in Figure 4D. The saturation curves obtained at increasing temperature when plotted as a function of the reduced parameter $\beta H/2kT$ do not superimpose, but are nested,[44] a behavior commonly observed for integer spin systems and associated with rhombic zero field splitting of the ground state non-Kramers doublet (*vide infra*). For any $S > {}^1/_2$, there can also be a contribution to the nesting from population of higher sublevels of the ground state. Comparison of the saturation curves measured on the 7700 cm^{-1} and 10400 cm^{-1} bands of the two-azide-bound complex (Figure 4, parts C and D) reveals that the 10400 cm^{-1} band shows rapid saturation, while the 7700 cm^{-1} band saturates noticeably more slowly, that is, at higher fields for the same temperature. This observation suggests that there are two different ground states, indicating that two different two-azide-bound species are present.

Analysis

A. Fully Reduced R2. Gaussian resolution of Figures 1A (CD) and 3A (MCD) show that reduced R2 has two low-energy bands (~5500 and 7000 cm^{-1}) and one high-energy band (~9300 cm^{-1}). The presence of three bands in the ligand field region indicates that the two Fe(II) atoms have different coordination environments, since a single Fe(II) atom cannot have more than two ligand field transitions above 5000 cm^{-1}.[37] A high-spin ferrous ion (d^6 electron configuration) has a ^5D ground state which is split into a triply degenerate $^5T_{2g}$ ground state and doubly degenerate ^5E_g excited state at $10Dq_{Oh}$ higher energy in an octahedral ligand field. For biologically relevant ligands such as N or O, the splitting 10Dq is on the order of 10000 cm^{-1}.[45] The ^5E_g state in a six-coordinate Fe(II) complex is generally split (Δ^5E_g) either by an excited-state Jahn–Teller distortion or by a static low-symmetry distortion in the ground

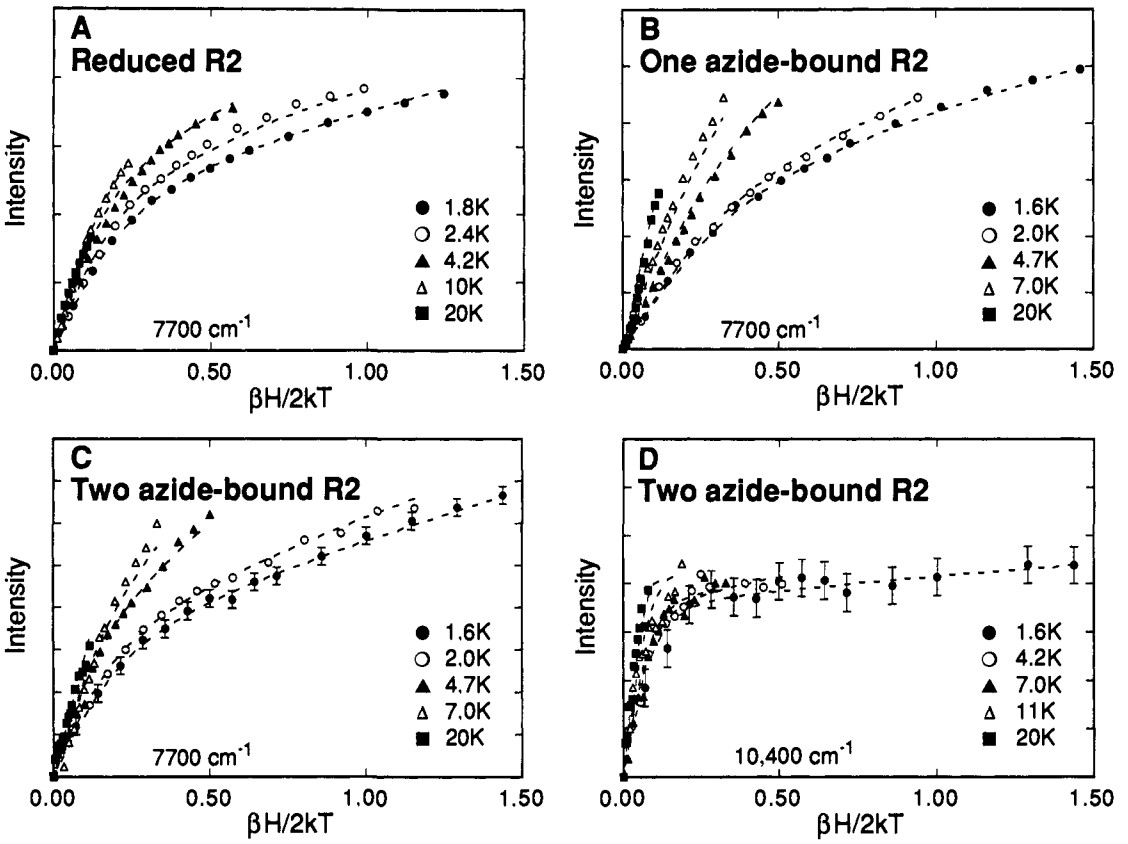

Figure 4. Saturation–magnetization behavior for (A) reduced R2 at 7700 cm^{-1}, (B) one-azide-bound R2 complex at 7700 cm^{-1}, (C) two-azide-bound R2 complex at 7700 cm^{-1}, and (D) two-azide-bound R2 complex at 10400 cm^{-1}. The MCD intensity amplitude for a range of magnetic fields (0–7.0 T) at a series of fixed temperatures is plotted as a function of $\beta H/2kT$. The fit to the VTVH MCD data (- - -) is for the parameters shown in Table 2 and was obtained as described in the text. The error bars for the lowest temperature points have been included and are representative of the error for all the data points. In the case of reduced R2 and the one-azide-bound R2 complex, the error bars for individual points are on the order of the symbol size used. Note that a subset of the data in this figure is plotted on an expanded scale in Figure 5.

state, resulting in a pair of absorption transitions split by ~2000 cm^{-1} and centered around 10000 cm^{-1}. Ligand field calculations on six-coordinate geometries have shown that the lowest energy band associated with a pseudooctahedral Fe(II) geometry is above 8100 cm^{-1}.[37] Removing one axial ligand from a tetragonally distorted octahedral complex leads to the formation of a square pyramidal five-coordinate complex and results in a larger Δ^5E_g splitting (~5000 cm^{-1}). A square pyramidal structure can be distorted into a trigonal bipyramidal structure via rearrangement along a C_{2v} or C_s coordinate. The two five-coordinate geometries are distinguishable; for a square pyramidal geometry the highest energy transition is $\geq$10000 cm^{-1}, while in a trigonal bipyramidal geometry the highest energy spin-allowed transition will be at <10000 cm^{-1}. In the limit of a large tetragonal elongation, one obtains a square planar four-coordinate complex. Distortion of the square planar structure along a D_{2d} coordinate leads to a tetrahedral geometry. A tetrahedral ligand environment will split the ferrous ^5D ground state by an energy of $10Dq_{Td} = -4/9(10Dq_{Oh})$, leading to a ^5E_g ground state and a $^5T_{2g}$ excited state. The spin-allowed ligand field transitions in a tetrahedral complex will occur at ~5000 cm^{-1}.

These correlations between d → d transitions and geometry provide a structural probe of the ferrous active site in RDPR. Reduced R2 only shows one transition higher than 8100 cm^{-1}, demonstrating that neither of the Fe(II) atoms is six-coordinate. The presence of one transition at ~9300 cm^{-1}, however, indicates that one Fe(II) atom is in a five-coordinate environment and suggests that the Fe(II) is distorted toward a trigonal bipyramidal structure. Since there are a minimum of two low-energy transitions observed, the second Fe(II) atom in the reduced R2 active site must be either five- or four-coordinate.

Variable-temperature variable-field MCD can be used to probe the ground state of high-spin Fe(II) active sites. As mentioned above, the saturation–magnetization curves in Figure 4 are nested with the high-temperature data offset from the low-temperature data. Such behavior is associated with rhombic zero-field splitting of the ground state doublet and arises from nonlinear field-induced mixing between the partners of the non-Kramers doublet.[44] In addition, at lowest temperature and highest fields the intensity increases linearly with increasing field. This intensity behavior reflects the presence of a B term since a pure C term will saturate at low temperature and high field.

The MCD intensity expression for a non-Kramers system which allows for the effects of linear B terms and the presence of excited states is given in eq 1:[46–48]

$$\Delta\epsilon = \sum_i \left\{ (A_{\mathrm{satlim}})_i \int_0^{\pi/2} \frac{\cos^2\theta \sin\theta}{\Gamma_i} (g_{\parallel_i}\beta H)\alpha_i \, d\theta + B_i H \gamma_i \right\} \quad (1)$$

where

(44) Thomson, A. J.; Johnson, M. K. *Biochem. J.* **1980**, *191*, 411.
(45) Lever, A. P. B. In *Inorganic Electronic Spectroscopy*; Elsevier: New York, 1984; p 458.
(46) Whittaker, J. W.; Solomon, E. I. *J. Am. Chem. Soc.* **1988**, *110*, 5329.
(47) McCormick, J. M. Ph.D. Thesis, Stanford University, 1991.
(48) Solomon, E. I.; Pavel, E. G.; Loeb, K. E.; Campochiaro, C. *Coord. Chem Rev.*, in press.

$$\Gamma_i = \sqrt{\delta_i^2 + (g_{\parallel_i}\beta H \cos\theta)^2}$$

$$\alpha_i = \frac{e^{-(E_i - \Gamma_i/2)/kT} - e^{-(E_i + \Gamma_i/2)/kT}}{\sum_j e^{-(E_j - \Gamma_j/2)/kT} + e^{-(E_j + \Gamma_j/2)/kT}}$$

$$\gamma_i = \frac{e^{-(E_i - \delta_i/2)/kT} + e^{-(E_i + \delta_i/2)/kT}}{\sum_j e^{-(E_j - \delta_j/2)/kT} + e^{-(E_j + \delta_j/2)/kT}}$$

In eq 1, which assumes pure xy polarization, $A_{\mathrm{satlim}i}$ is the C term intensity of state i, E_i is the energy above the ground state ($E_1 = 0$), δ_i is the zero-field splitting of the ith non-Kramers doublet, θ is the angle between $g_{\parallel_i}$ and the external magnetic field H, β is the Bohr magneton, k is the Boltzmann constant, T is the absolute temperature, and B_i is the B term contribution. Each B_i will be the sum of several B terms arising from field-induced mixing of the ith state with high-lying excited states as well as with other sublevels within the ground state spin manifold for fields not along the z axis. Values of $A_{\mathrm{satlim}i}$, δ_i, and $g_{\parallel_i}$ are obtained using a simplex routine to fit the experimental magnetization data sets in Figure 4, which consist of the MCD intensity, temperature, and the applied magnetic field.

Ground state analysis of the pumped helium temperature data of reduced R2 (Figure 4A) using one non-Kramers doublet indicates that there is a doublet lowest in energy which has a $g_{\parallel} = 9.3$ and $\delta = 4.2$ cm^{-1}. In order to validate the assumption made in eq 1, namely, that the electronic transitions are purely xy-polarized, the contribution of a z-polarized transition ($M_z/M_{xy} > 0$) and the consequent effects of a non-zero $g_\perp$ value have been investigated. Allowing for the effects of z polarization[46,48] in the analysis decreases the $g_{\parallel}$ value and may slightly change the δ value but does not significantly improve the quality of the fit relative to the fit from eq 1. The ground and excited state parameters for reduced R2, including the additional parameters $g_\perp$ and M_z/M_{xy}, are given in Table 2. It should be noted that the fit to the VTVH data is most sensitive to $g_{\parallel}$ and δ,[48] and the error bars given in Table 2 represent the deviations observed. The B term, $g_\perp$, and M_z/M_{xy} values, on the other hand, are less rigorously defined, and Table 2 lists the values obtained in the best fit to the data. However, the interpretation of the VTVH MCD analysis relies solely on the parameters that can be accurately determined, $g_{\parallel}$ and δ.

Application of eq 1 to the reduced R2 saturation data taken from 1.6 to ~4.2 K provides a fit with a single non-Kramers doublet having the ground state parameters given in Table 2. At higher temperatures the fit consistently overestimates the intensity of the signal, indicating the presence of at least one low-lying excited state (Figure 5A). The effects of excited states ($i > 1$) on the MCD saturation–magnetization curves were included in the fit by holding the best fit ground state parameters constant and allowing all parameters associated with a single excited state (A_{satlim}, B, $g_{\parallel}$, δ, and energy) to float. In order to fit the high-temperature variable-field saturation data, reduced R2 requires the presence of an excited state at ~6.0 cm^{-1}. We were able to obtain a number of good fits to the data; thus the error bars for the excited state given in Table 2 were obtained by averaging the results of these fits.

It should be noted that the ground state parameters obtained in the fits of the VTVH data of reduced R2 are similar to those

Table 2. MCD Parameters for the Ground State and Lowest Excited States of Reduced R2, One-Azide-Bound R2, and Two-Azide-Bound R2

	reduced R2	one-azide-bound R2	two-azide-bound R2	
	7700 cm^{-1}	7700 cm^{-1}	7700 cm^{-1}	10400 cm^{-1}
$g_{\parallel}$	9.3 ± 0.7	3.9 ± 0.3	9.4 ± 0.5	16.0 ± 0.5
δ (cm^{-1})	4.2 ± 0.4	<1.0	3.3 ± 0.5	<1.0
$g_\perp$	0.66	0.43	1.55	1.0
M_z/M_{xy}	0.88	1.61	2.63	0.12
% B	~4.0	~4.0	~7.0	~1.5
ES (cm^{-1})	6.0 ± 0.8	8.0 ± 2.0	12.0 ± 2.0	15.0 ± 2.0

of monomeric Fe(II) complexes.[49] The ground state of a high-spin ferrous center can be described as an $S = 2$ spin manifold which undergoes axial zero-field splitting into $M_s = \pm 2, \pm 1, 0$ components. When the non-Kramers $M_s = \pm 2$ doublet is lowest in energy, an effective g value of 8.00 (assuming the molecular g values are 2.00) is obtained for the ground state.[50] However, the active site of ribonucleotide reductase consists of a binuclear non-heme iron center. Therefore, we consider the electronic structure of the ground state of a coupled binuclear ferrous site in order to determine whether a spin-coupled system can produce a ground state having the observed parameters. The electronic structure of the ground state is described by the spin Hamiltonian given in eq 2 where the subscripts denote the different Fe(II) ions.[36]

$$\begin{aligned}\hat{\mathcal{H}} = -2J\hat{S}_1\cdot\hat{S}_2 + D_1\left(\hat{S}^2_{z1} - \tfrac{1}{3}S(S+1)\right) + E_1(\hat{S}^2_{x1} - \hat{S}^2_{y1}) + \\ D_2\left(\hat{S}^2_{z2} - \tfrac{1}{3}S(S+1)\right) + E_2(\hat{S}^2_{x2} - \hat{S}^2_{y2}) + g_{z1}\beta H_z\hat{S}_{z1} + \\ g_{x1}\beta H_x\hat{S}_{x1} + g_{y1}\beta H_y\hat{S}_{y1} + g_{z2}\beta H_z\hat{S}_{z2} + \\ g_{x2}\beta H_x\hat{S}_{x2} + g_{y2}\beta H_y\hat{S}_{y2} \quad (2)\end{aligned}$$

Equation 2 includes the exchange coupling (J) between the iron atoms, the axial ($D_{1,2}$) and rhombic ($E_{1,2}$) zero-field splitting (ZFS) parameters for each iron (1,2), and the Zeeman terms ($g_{z1}\beta H_z S_{z1}$, etc.). This Hamiltonian operates on an uncoupled basis set ($|S_1,M_{s1}, S_2,M_{s2}\rangle$, $M_s = 2,1,0,-1,-2$) yielding a 25 × 25 matrix. Diagonalization of this matrix in zero field yields energies and spin wave functions of the binuclear ground state.

As a first approximation, axial symmetry was assumed ($E_1 = E_2 = 0$) and the D values for each iron atom were set equal. The calculation was then performed over a range of J values for a fixed value of D ($D_1 = D_2 = -15$ cm^{-1}), and the results are presented in Figure 6A. The center of Figure 6A shows the limiting case with large ZFS and no exchange coupling. These states are labeled by the uncoupled basis functions (M_{s1}, M_{s2}). These levels are split as the iron atoms begin to interact. The right side of Figure 6A shows two $S = 2$ ions that are ferromagnetically coupled ($J > 0$ cm^{-1}) to produce a $|4, \pm 4\rangle$ (S_{Tot}, $|M_s|$) non-Kramers doublet ground state with the $|4, \pm 3\rangle$ doublet or the $|4, 0\rangle$ and $|3, 0\rangle$ singlet states at higher energy depending on the magnitude of J. Alternatively, if the iron atoms are antiferromagnetically coupled ($J < 0$ cm^{-1}), the ground state is a singlet for any value of J (Figure 6A left).[51] On the basis of Figure 6A, the $|4, \pm 4\rangle$ ground state of a ferromagnetically coupled [Fe(II)Fe(II)] center would produce a $g_{\parallel} = 16$, while the $|0, 0\rangle$ ground state would not show MCD C term intensity at lower temperatures.

(49) Solomon, E. I.; Zhang, Y. *Acc. Chem. Res.* **1992**, *25*, 343.

(50) Abragam, A.; Bleaney, B. *Electron Paramagnetic Resonance of Transition Ions*; Dover Publications: New York, 1970.

(51) It should be noted that Figure 6A can also be used to describe a system with positive axial ZFS ($D > 0$ cm^{-1}) for both Fe(II) atoms by reversing the energy scale such that the $|0,0\rangle$ level is the ground state for both ferromagnetic and antiferromagnetic coupling.

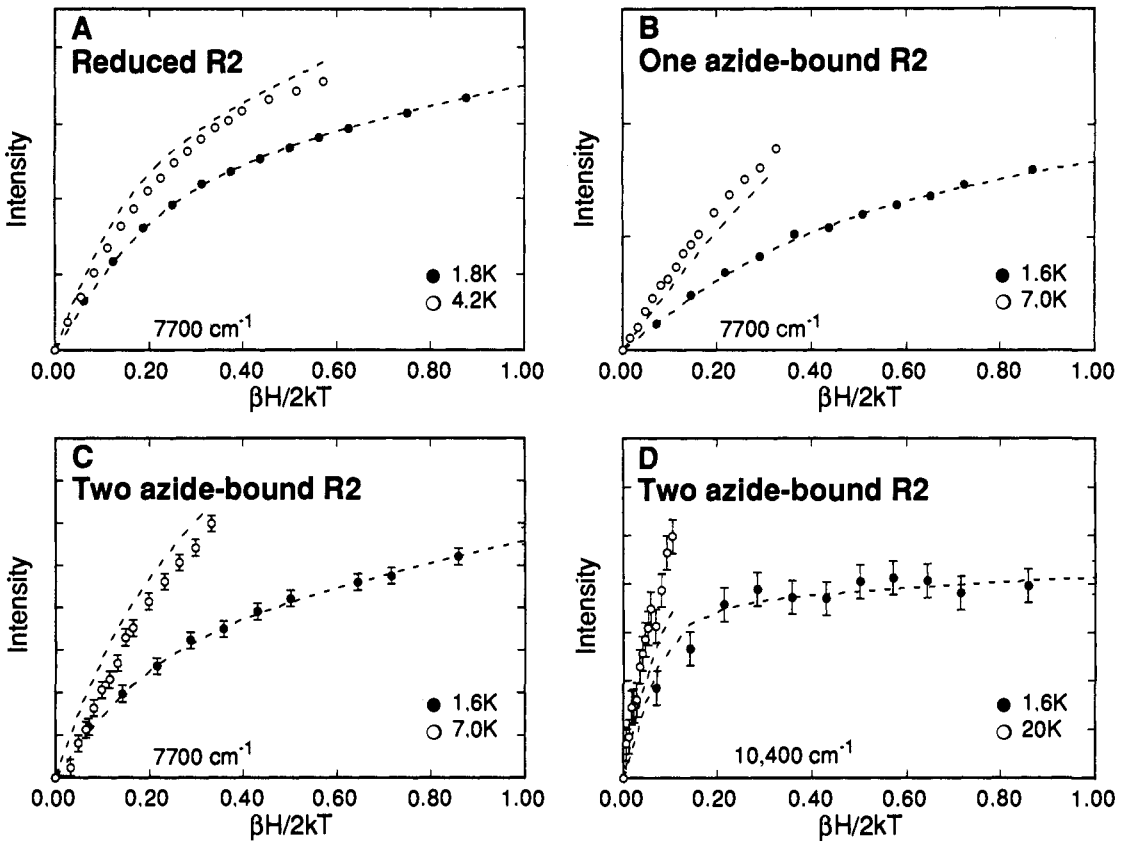

Figure 5. VH MCD (0.0−7.0 T) at 7700 cm^{-1} for (A) reduced R2 at 1.8 and 4.2 K, (B) the one-azide-bound R2 complex at 1.6 and 7.0 K, (C) the two-azide-bound R2 complex at 1.6 and 7.0 K, and at 10400 cm^{-1} for (D) the two-azide-bound R2 complex at 1.6 and 20 K. The dashed curve represents the fit for an isolated non-Kramers doublet ground state. Higher temperature data cannot be accurately fit with the same parameters as the ground state. Error bars have been included; in the case of reduced R2 and the one-azide-bound R2 complex the error bars for individual points are smaller than the symbol size used.

Inclusion of a rhombic perturbation on the energy diagram in Figure 6A (i.e., E_1 and E_2 are non-zero in eq 2) gives Figure 6B for $D_1 = D_2 = -15$ cm^{-1} and $E_1/D_1 = E_2/D_2 = 1/3$ (the rhombic limit). Any remaining degeneracies are removed when E is non-zero, as the $M_s = \pm n$ doublets are split and the wave functions mix. The VTVH MCD parameter δ in eq 1 is a measure of the rhombic splitting of an M_s ground state doublet. From Figure 6B it is evident that at the rhombic limit, ferromagnetic coupling (right side of Figure 6B) produces a $M_s = \pm 4$ ground state doublet which would have $g_{\|} = 16$, while antiferromagnetic coupling results in a MCD inactive singlet ground state (left side of Figure 6B). In light of the spin Hamiltonian results presented above, the saturation−magnetization ground state parameters for reduced R2 summarized in Table 2 cannot be explained in terms of two ferrous atoms having D values of the same magnitude and sign.

If we allow the D values to become unequal in magnitude but retain the same sign, the $|4, \pm 4\rangle$ ground state for $J > 0$ cm^{-1} in Figure 6A and the $|0, 0\rangle$ ground state for $J < 0$ cm^{-1} are maintained. Alternatively, when the D values associated with each ferrous atom become opposite in sign, the ground state energy level diagram changes significantly. A representative energy diagram obtained in this case is shown in Figure 6C. Here $D_1 = -10$ cm^{-1}, $D_2 = +5$ cm^{-1}, and J is varied from −5 to 5 cm^{-1}. The center of Figure 6C shows the limiting case with no exchange coupling. These states are labeled by the uncoupled basis functions (M_{s1}, M_{s2}). The levels are split as the Fe(II) atoms begin to interact ($|J| > 0$ cm^{-1}). If the iron atoms are ferromagnetically coupled, two different ground state doublets are possible ($|M_s| = 2$ and $|M_s| = 3$) depending on the relative magnitude of the exchange coupling, as shown at the lower right of Figure 6C. In the case of antiferromagnetic coupling (Figure 6C left), three different ground states are possible; namely, $|M_s| = 2$, $|M_s| = 1$, and $|M_s| = 0$, respectively, for increasing values of the antiferromagnetic coupling. Additional diagrams are required for different values of D_1 and D_2; however, there are a few observations that should be made. At $J = 0$ cm^{-1}, the energy separation between the ground $|\pm 2, 0\rangle$ and first excited $|\pm 2, \pm 1\rangle$ levels is equal to the magnitude of the mononuclear $+D$ ZFS value. This separation leads to ground state energy level crossings at higher J values. The $-D$ ZFS parameter does not have a large effect on the ground state level crossings; however, a decrease in the magnitude of $-D$ compresses the entire ground state energy diagram. Lastly inclusion of a rhombic perturbation on the energy diagram in Figure 6C removes all degeneracies and leads to mixed wave functions. The ground states are primarily $M_s = \pm 2$ or ± 1 doublets, which split dramatically in a rhombic environment. This increased splitting is reflected in the higher values of δ for these energy levels. The best fit to the VTVH MCD data of reduced R2 gives a $g_{\|} = 9.3$ and $\delta = 4.2$ cm^{-1}. An $M_s = \pm 2$ non-Kramers ground state doublet would be consistent with these parameters. As presented above, when D_1 and D_2 are unequal in sign an $|M_s| = 2$ ground state can be obtained for both weak ferromagnetic and weak antiferromagnetic coupling (Figure 6C). On the basis of the magnitude of D_1 and D_2, a range of J values can be determined.

From the ligand field transitions observed in the CD and MCD spectra of reduced R2, it was concluded that the [Fe(II)-Fe(II)] active site consists of one five- and one five- or four-coordinate iron atom. We favor four-coordinate for the second Fe(II) for a number of reasons. First, binding one azide to the

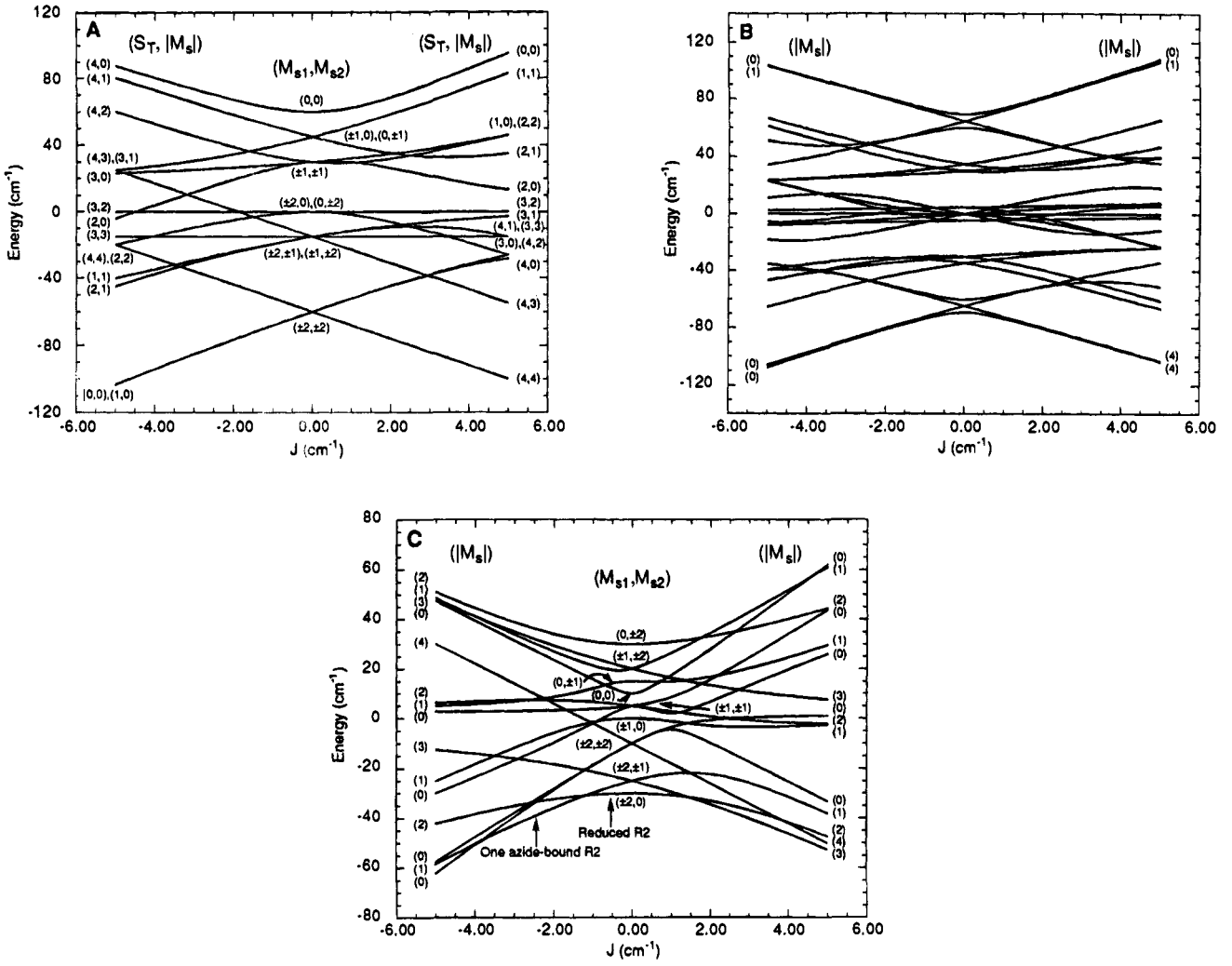

Figure 6. Correlation diagram of the energy levels of the binuclear ferrous ground state including exchange coupling and single-site ZFS. In (A) the axial ZFS parameters (D) on the two iron atoms are held constant and are constrained to be equal ($D_1 = D_2 = -15$ cm^{-1}), and the exchange coupling (J) is varied from -5 to 5 cm^{-1}. The central portion gives the pure ZFS limit with states labeled with M_s values for each uncoupled Fe(II) (M_{s1}, M_{s2}). The right side describes a ferromagnetic interaction ($J > 0$) between the ferrous atoms, and the left side shows an antiferromagnetic interaction ($J < 0$). The spin Hamiltonian used for calculating the levels is given in eq 2, with $E_1 = E_2 = 0$. (B) gives the energy levels of the binuclear ferrous ground state described in (A) at the rhombic limit of $E/D = 1/3$. In (C) the axial ZFS parameters on the two iron atoms are different in magnitude and opposite in sign ($D_1 = -10$ cm^{-1}, $D_2 = 5$ cm^{-1}), and the exchange coupling is varied from -5 to 5 cm^{-1}.

active site perturbs the ligand field of only one ferrous center and results in one four- and one six-coordinate Fe(II) atom (*vide infra*). Second, the VTVH MCD data of reduced RDPR requires the axial ZFS parameters of the two Fe(II) sites to be of opposite sign based on the spin Hamiltonian results presented above. A positive value of D would be obtained in the case of a flattened tetrahedron (*vide infra*) or in a square pyramidal complex containing a strong axial bond. The latter possibility, however, would be characterized by a short metal−ligand bond which is not observed in reduced RDPR.[35,52] In addition, a strong-axial square pyramidal complex would not produce ligand field transitions consistent with those observed.[48] Third, crystallographic data on fully reduced R2 shows two four-coordinate Fe(II) sites.[35,52]

We therefore treat the reduced R2 active site as consisting of one five-coordinate Fe(II) atom in a distorted trigonal bipyramidal environment and one four-coordinate Fe(II) atom in a distorted tetrahedral environment. A positive axial ZFS parameter D would correspond to a distorted tetrahedron which has been flattened along the z axis.[53] Equation 3 gives an expression for D in terms of the energy difference (Δ') between the ground state and lowest component of the $^5T_2$ excited state and the spin−orbit coupling parameter (λ).[53,54]

$$D = \frac{+3\lambda^2}{\Delta'} \tag{3}$$

On the basis of the position of the two low-energy features in reduced R2, and using -80 cm^{-1} as the spin−orbit coupling value,[48] a D value on the order of $+4$ cm^{-1} is calculated. A five-coordinate Fe(II) atom in a trigonal bipyramidal environment will have negative axial ZFS,[55] with $-D$ ranging from -5 to -15 cm^{-1}.[56] Therefore, the parameters used to calculate the ground state energy level diagram in Figure 6C are appropriate for reduced R2 and lead to the conclusion that $-1.25 < J < 1.25$ cm^{-1}, $D_1 \approx -10$ cm^{-1}, and $D_2 \approx 5$ cm^{-1}. The results from the spin Hamiltonian analysis are summarized in Table 3 and graphically presented in Figure 6C.

The weak coupling is consistent with the SQUID magnetic susceptibility data of reduced R2.[32] However, the authors

(52) Atta, M.; Nordlund, P.; Åberg, A.; Eklund, H.; Fontecave, M. *J. Biol. Chem.* **1992**, *267*, 20682.

(53) Hartmann-Boutron, F.; Imbert, P. *J. Appl. Phys.* **1968**, *39*, 775.
(54) Varret, F.; Hartmann-Boutron, F. *Ann. Phys.* **1968**, *3*, 157.
(55) Wood, J. S.; Greene, P. T. *Inorg. Chem.* **1969**, *8*, 491.
(56) Rudowicz, C. *Acta Phys. Pol.* **1975**, *A47*, 305.

Table 3. Spin Hamiltonian Parameters for Fully Reduced R2, One-Azide-Bound R2, and Two-Azide-Bound R2

			two-azide-bound R2	
	reduced R2	one-azide-bound R2	component I (7700 cm^{-1} band)	component II (10400 cm^{-1} band)
J (cm^{-1})	-0.5 ± 0.1	-2.5 ± 1.0	$-2.0 < J < 2.0$	1.0 ± 0.5
D_1 (cm^{-1})	-10.0 ± 2.0	-13.0 ± 2.0	-10.0 ± 5.0	-10.0 ± 5.0
D_2 (cm^{-1})	$+4.0 \pm 1.0$	$+4.0 \pm 1.0$	$+4.0 \pm 1.0$	-10.0 ± 5.0

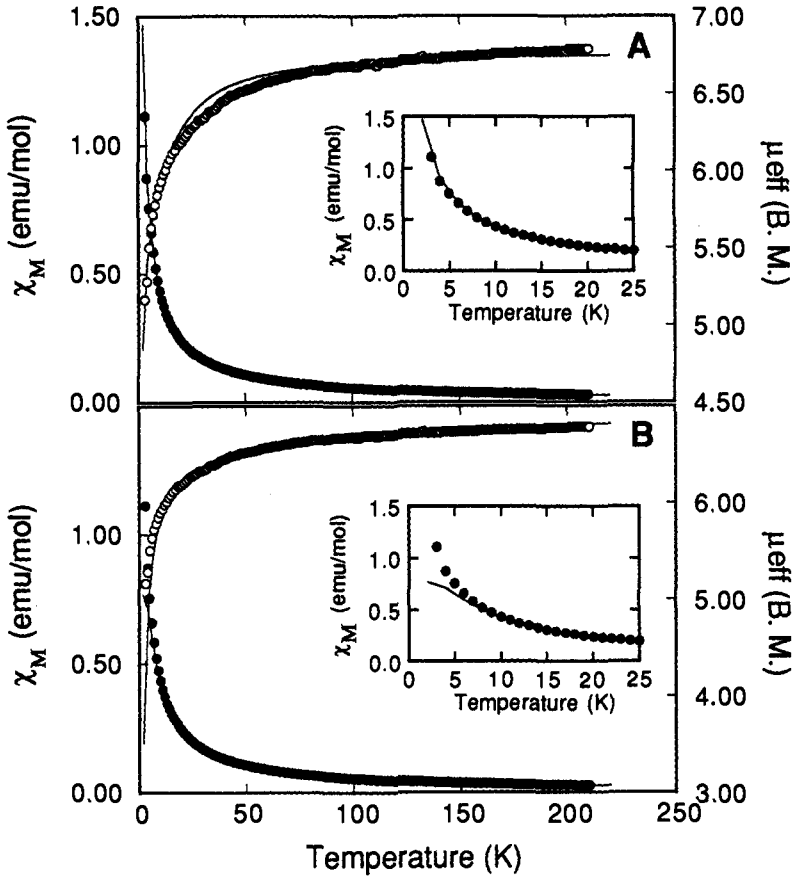

Figure 7. Magnetization of reduced R2 at 0.5 T over a temperature range of 2−300 K. Data are plotted as molar susceptibility (χ_M; ●) and effective magnetic moment (μ_{eff}; ○) versus temperature. The data have been adapted from ref 32. (A) A least-squares best fit to the data (—) using eq 2 which gives $J = -0.4$ cm^{-1}, $D_1 = -10.4$ cm^{-1}, $D_2 = 4.4$ cm^{-1}, $E_{1,2}/D_{1,2} = 0.33$, and $g_{ave} = 1.96$. (B) Fit to the data using the parameters given in ref 32 ($J = 0.3$ cm^{-1}, $D_1 = D_2 = 9.8$ cm^{-1}, $E_{1,2}/D_{1,2} = 0$). The low-temperature regions of the χ_M data from (A) and (B) are shown in the respective figure insets.

interpreted the magnetization data in terms of two equivalent Fe(II) atoms and obtained a best fit for $J = 0.3$ cm^{-1} (i.e., ferromagnetic), $D_1 = D_2 = 9.8$ cm^{-1} and $E/D = 0.0$. In light of the MCD saturation−magnetization results presented above, it is necessary to reevaluate the earlier fitting of the susceptibility data. Magnetization data from ref 32 are plotted as molar susceptibility (●, χ_M) versus temperature in Figure 7. Also included in Figure 7 is the effective magnetic moment (○, μ_{eff}) for reduced R2 as a function of temperature.[57] The solid lines shown in Figure 7A are least-squares fits calculated by diagonalization of the 25 × 25 spin Hamiltonian of eq 2 under the assumption of coaxial D tensors. A best fit was obtained with $J = -0.44$ cm^{-1}, $D_1 = -10.4$ cm^{-1}, $D_2 = 4.4$ cm^{-1}, $E_{1,2}/D_{1,2} = 1/3$, and $g_{ave} = 1.96$. These values correspond well to those obtained from VTVH MCD measurements under the same model constraints. The solid lines in Figure 7B show the fit to the magnetization data using the fitting parameters from ref 32. The fit obtained using these parameters describes the high-temperature molar susceptibility data well but underestimates the magnitude of the low-temperature data (inset of Figure 7B). Considering that magnetic susceptibility is most sensitive at low temperature, the increased deviation of the fit illustrated in Figure 7B at these temperatures is reflected by an overall increase in χ^2 (the goodness of fit parameter) of 500% when compared to the fit in Figure 7A.

In summary, the fully reduced R2 active site appears to consist of one five-coordinate Fe(II) atom in a trigonal bipyramidal geometry and one four-coordinate Fe(II) atom in a distorted tetrahedral geometry. The ferrous atoms are weakly antiferromagnetically coupled ($J = -0.5 \pm 0.1$ cm^{-1}) and have unequal D values consistent with iron atoms in different coordination environments. Furthermore, the D values must have opposite signs, and it is reasonable from ligand field theory that the Fe(II) center with the negative value of D be associated with the five-coordinate Fe(II) site, while the positive value of D is associated with the four-coordinate Fe(II) center.

B. One-Azide-Bound R2. The CD spectrum of fully reduced R2 changes significantly upon formation of the first azide-bound R2 complex (Figure 1, parts A and B). The one-azide-bound species shows two high- and two low-energy bands.

(57) The molecular g values were scaled to the 220 K value of μ_{eff} (B.M.). O'Connor, C. J. *Prog. Inorg. Chem.* **1982**, *29*, 203.

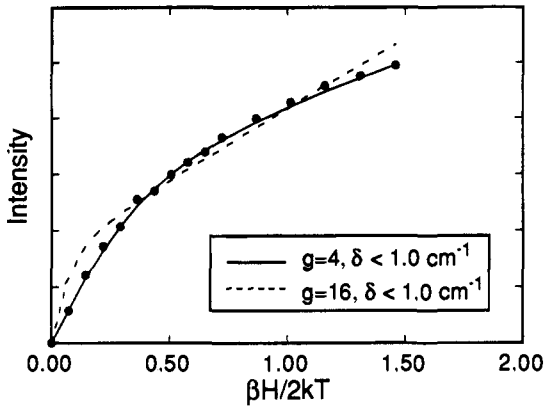

Figure 8. Saturation−magnetization curve for the one-azide-bound R2 complex at 7700 cm^{-1} and 1.6 K. Ground state fit to the VTVH data using the parameters predicted by EPR (ref 34): $g_{||} = 16$ and $\delta <$ 1.0 cm^{-1} (- - -) and by MCD; $g_{||} = 4.0$ and $\delta <$ 1.0 cm^{-1} (—). The fits are for an isolated non-Kramers doublet ground state.

There are two coordination assignments consistent with the observed ligand field transitions; namely, two five-coordinate Fe(II) atoms or one six- and one four-coordinate Fe(II) atom. Comparison of the MCD spectra of reduced R2 and the one-azide-bound complex (Figure 3, parts A and B) reveals that there is no significant change in band position; however, the intensity of the ~5200 cm^{-1} band has increased. Thus the CD intensity decreases while the MCD intensity increases in the same region, suggesting that a MCD active negative band has been eliminated with azide binding to the reduced R2 active site. The elimination of a low-energy band and simultaneous appearance of a new high-energy ligand field transition in the CD spectrum suggest that the coordination environment of one Fe(II) atom is significantly perturbed upon formation of the one-azide-bound complex. Since the two low-energy features at ~5200 and 7500 cm^{-1} remain largely unperturbed and a third low-energy band appears to be shifted to higher energy, the binuclear ferrous active site in the one-azide-bound complex is best described as having one six- and one four-coordinate Fe(II) center.

The ground state properties of the one-azide-bound R2 complex can be obtained from the VTVH MCD data shown in Figure 4B. Fitting the saturation−magnetization data for the one-azide-bound complex yields the ground state parameters $g_{||} = 4.0 \pm 0.3$ and $\delta <$1.0 cm^{-1}. Allowing for effects of z polarization in the analysis did not improve the fit, indicating that the data do not require the additional parameters and that the transition at 7700 cm^{-1} is mostly xy-polarized. At temperatures above ~5.0 K the non-Kramers ground state contribution alone does not fit the data, indicating the population of an excited state (Figure 5B). To fit the higher temperature data, the saturation analysis (eq 1) requires an excited state at ~8.0 cm^{-1}. The fit to the complete VTVH MCD data is included in Figure 4B.

The ground state properties of the one-azide-bound R2 complex have also been investigated by EPR spectroscopy.[34] In this study, EPR titrations with azide were performed which showed that anaerobic addition of N_3^- to reduced R2 elicits an EPR signal at g_{eff} ~17.0. Since reduced R2 is effectively EPR silent, the authors suggested that azide binding converts the EPR-silent [Fe(II)Fe(II)] center into EPR-active ferromagnetically coupled sites. We have attempted to fit our VTVH MCD data with the g value determined from EPR spectroscopy; however, as shown in Figure 8 $g_{||} = 16.0$ and $\delta <$ 1.0 cm^{-1} do not fit the data.[58] It should be noted that while there are some differences in the conditions betweeen the two experiments (higher glycerol and buffer concentrations for MCD), the best fit parameters for the MCD data do predict that the one-azide-bound R2 complex is an EPR detectable integer spin system as observed in ref 34 but with a different spectral assignment.

The results of the saturation−magnetization analysis and the observation of an EPR signal can be combined to produce a model for the ground state of the one-azide-bound complex. The magnetization behavior requires the presence of a ground state non-Kramers doublet,[46] while EPR dictates that the zero-field splitting of this doublet will be small ($\delta <$ 1.0 cm^{-1}).[58] Thus the experimental $g_{||}$ of ~4.0 and $\delta <$ 1.0 cm^{-1} are in accord with the constraints described. The parameters required to fit the saturation-magnetization data of the one-azide-bound R2 complex are given in Table 2.

A $g_{||}$ of 4.0 suggests that the lowest component of the ground state is a $M_s = \pm 1$ non-Kramers doublet. As shown in Figure 6C, a ± 1 doublet ground state for a Fe(II) dimer can be obtained if the iron centers are antiferromagnetically coupled and the axial ZFS values of the iron atoms are oppositely signed. When $-1.25 < J < -3.75$ cm^{-1}, the ground state can be described as a $|M_s| = 1$ doublet. It should be noted, however, that the range of J will be affected by the magnitudes of D_1 and D_2 (in Figure 6C these are set at $D_1 = -10$ and $D_2 = +5$ cm^{-1}).

From the ligand field analysis of the CD and MCD spectra of the one-azide-bound R2 complex, the active site consists of one four- and one six-coordinate Fe(II) atom. Since the addition of azide to fully reduced R2 does not greatly perturb the d → d spectral features of the four-coordinate site, this Fe(II) can still be described as distorted tetrahedral having a positive axial ZFS (*vide supra*). The second Fe(II) center has become six-coordinate, suggesting that the negative axial ZFS parameter associated with this site has increased. From ligand field theory the largest reasonable magnitude for the ZFS should be observed in a distorted six-coordinate Fe(II) site and is experimentally found to be approximately −15 cm^{-1}.[56] Increasing the magnitude of D_1 to −15 cm^{-1} limits the range of J from −1.25 to −4.0 cm^{-1} in order to have a ± 1 doublet ground state. Higher values of $|J|$ lead to a $M_s = 0$ ground state. The results from the spin Hamiltonian analysis are summarized in Table 3 and graphically indicated in Figure 6C.

In summary, binding azide to reduced R2 causes the appearance of a high-energy band at ~10500 cm^{-1}. The CD and MCD data are explained by one iron having a six-coordinate geometry. This suggests that the five-coordinate Fe(II) ion in reduced R2 binds a single azide to become six-coordinate. The azide does not appear to bridge in that the second Fe(II) atom stays four-coordinate. The formation of the one azide-bound complex also affects the electronic structure of the binuclear ferrous ground state by raising the magnitude of the negative ZFS and by increasing the exchange coupling from -0.5 ± 0.1 cm^{-1} to -2.5 ± 1.0 cm^{-1}. This increase in antiferromagnetism is small and would also not be consistent with an azide bridge since one might expect a negative J greater than −10 cm^{-1} for a Fe(II)−N_3−Fe(II) complex based on the $J \approx -500$ cm^{-1} for μ-1,3 azide bridged binuclear copper systems.[59-61] The change in exchange

(58) Hendrich, M. P.; Pearce, L. L.; Que, L.; Chasteen, N. D.; Day, E. P. *J. Am. Chem. Soc.* **1991**, *113*, 3039.

(59) Comarmond, J.; Plumeré, P.; Lehn, J.-M.; Agnus, U.; Louis, R.; Weiss, R.; Kahn, O.; Morgenstern-Badarau, I. *J. Am. Chem. Soc.* **1982**, *104*, 6330.

(60) Bkouche-Waksman, I.; Biollot, M.-L.; Kahn, O.; Sikorav, S. *Inorg. Chem.* **1984**, *23*, 4454.

(61) A binuclear Cu−N_3^-−Cu system has only one possible exchange pathway. In the case of a binuclear [Fe(II)Fe(II)] complex, there are 16 possible pathways. Therefore, dividing the J value obtained from the copper system by 16 gives an estimate for the exchange coupling of an Fe−N_3^-−Fe complex.

coupling, however, is consistent with the fact that reduced R2 has a $M_s = \pm 2$ ground state while the one-azide-bound complex has a ± 1 ground state (Figure 6C). The ground state differences also reflect the fact that reduced R2 does not exhibit an EPR signal while the one-azide-bound complex is EPR active. The observation of an EPR signal requires that the zero-field splitting of the ground state doublet be <1.0 cm^{-1}. For a weakly coupled antiferromagnetic binuclear ferrous cluster with opposite signs of D, δ is most sensitive to the E/D ratio of the Fe(II) atom associated with the negative axial ZFS and a δ value of less than 1.0 cm^{-1} is obtained if the $-D$ Fe(II) atom has an $E/D < 0.1 \pm 0.02$.

C. Two-Azide-Bound R2. Comparison of the CD spectra of the one-azide-bound and two-azide-bound complexes (Figure 1, parts B and C, respectively) shows that the low-energy CD transitions decrease slightly in intensity when the second azide binds to the reduced R2 active site. In contrast, a large change in the MCD spectrum is observed when the two-azide-bound R2 complex is formed. Comparison of Figure 3, parts B and C reveals that the intensities of the low energy bands have decreased and that a new negative higher energy transition is observed.

VTVH MCD data for the 7700 cm^{-1} and 10400 cm^{-1} bands of the two-azide-bound complex (Figure 4, parts C and D, respectively) indicate that each band is associated with a ground state that has a different g value. Best fit analysis of the VTVH MCD data from the band at 7700 cm^{-1} indicates that there is a doublet lowest in energy which has $g_{||} = 9.4$ and $\delta = 3.3$ cm^{-1}, while analysis of the VTVH MCD data from the 10400 cm^{-1} band indicates that there is a doublet lowest in energy which has a $g_{||} = 16.0 \pm 0.5$ and $\delta < 1.0$ cm^{-1}. Allowing for the effects of z polarization in the analysis did not change the fits. These results, therefore, indicate that there are two different components of the two-azide-bound form present in the site.

On the basis of the intensity decrease in the low-energy region of the MCD spectrum, the second azide appears to bind to the four-coordinate Fe(II) atom of the one-azide-bound complex to produce a five-coordinate Fe(II) site in one component of the two-azide-bound system. The corresponding appearance of a high-energy negative MCD band (see Figure 3C) supports this assignment. The second Fe(II) site likely remains six-coordinate as is evidenced by the fact that the two negative CD bands at 9000 and 10200 cm^{-1} remain the same in the one- and two-azide-bound R2 complexes (Figure 1). The fact that the 5300 and 7500 cm^{-1} features in the CD and MCD do not completely go away indicates that the second [Fe(II)Fe(II)] species present must have one four-coordinate ferrous site. It is important to note that this is not simply a residual of the one-azide-bound form as its $g_{||}$ value is 9, not the $g_{||} = 4$ of the former species. The geometry of the second Fe(II) atom in this $g \sim 9$ component cannot be definitively established on the basis of the available data; however, we favor a six-coordinate environment since the high-energy features in the CD spectrum of the two-azide-bound form have not decreased in intensity when compared to the one-azide-bound complex.

As discussed above, the ground state best fit to the 7700 cm^{-1} VTVH MCD data of the two-azide-bound R2 gives a $g_{||} = 9.4$ and $\delta = 3.3$ cm^{-1}. At temperatures above $\sim$7.0 K the non-Kramers ground state contribution alone does not fit the data, indicating the population of an excited state (Figure 5C). To fit the higher temperature variable-field data, an excited state at $\sim$13 cm^{-1} must be included in the saturation analysis. An $M_s = \pm 2$ non-Kramers doublet ground state would be consistent with the g value calculated. As shown in Figure 6C, a ± 2 ground state will result if D_1 and D_2 are opposite in sign and the exchange coupling is either weakly ferro- or weakly antiferromagnetic. The range of J will be limited by the relative magnitudes of D_1 and D_2. From the ligand field transitions observed in the CD and MCD spectra of this component of the two-azide-bound R2 system, the $g \sim 9$ value is associated with a band of a four-coordinate Fe(II) atom. This ferrous center, therefore, should have a positive D value of approximately 5 cm^{-1} (*vide supra*). The second Fe(II) atom is either five- or six-coordinate, giving a range for $-D$ from -5 to -15 cm^{-1}. These parameters indicate that J must be between -2.0 and 2.0 cm^{-1} in order to have a ± 2 ground state doublet (Figure 6C).

In contrast, ground state analysis of the pumped helium temperature data of the 10400 cm^{-1} band indicates that there is a doublet lowest in energy which has $g_{||} = 16.0 \pm 0.5$ and $\delta < 1.0$ cm^{-1}. Thus the site is ferromagnetically coupled with a $|4, \pm 4\rangle$ (S_{Tot}, M_{sTot}) doublet lowest in energy (see Figure 6A) consistent with EPR results.[34] The ground state parameters given in Table 2 can be used to fit data up to 11 K. At higher temperatures, the fit underestimates the intensity of the signal, indicating the presence of at least one low-lying excited state (Figure 5D). There are two possible excited states: a MCD active state (4, ± 3) and a MCD inactive state (4, 0; 3, 0) (Figure 6A, right side). The (4, ± 3) doublet has an associated $g_{||}$ value of 12, while for the (4, 0; 3, 0) doublet $g_{||} \sim 0$. Both doublets were included as excited states in eq 1 {(4, ± 3): $|A_2| > 0$, $g_{||} = 12$; (4, 0; 3, 0): $A_3 = 0$, $g_{||} = 0$}, allowing all the other parameters (B_i, δ_i, energy (E_i)) to vary. Best fit values were obtained if the MCD inactive doublet is at $\sim$15 cm^{-1} and the MCD active doublet is at $\sim$30 cm^{-1}. The fit to the complete set of MCD saturation−magnetization data with these excited states is given in Figure 4D. Including only the (4, ± 3) or the (4, 0; 3, 0) doublet as the excited state gave a worse fit to the data (χ^2 increased by 40%).

The saturation−magnetization ground state parameters for the species with the 10400 cm^{-1} band in the two-azide-bound R2 form summarized in Table 2 were used to determine the spin Hamiltonian parameters in eq 2. The first excited state for this component of the two-azide-bound complex lies at 15 cm^{-1} and is MCD inactive (i.e., the (4, 0; 3, 0) doublet in Figure 6A), thus limiting the range of possible J, D solutions. In order to extract the ground state parameters, all values of D and J resulting in an excited state 15−30 cm^{-1} above the ground state were located. These results are given in Figure 9A, where the $- \cdot -$ and $- \cdots -$ curves bracket the values of J and D required to reproduce the experimental splitting range of 15−30 cm^{-1}. Similarly, VTVH MCD fits determined the value for the zero-field splitting of the non-Kramers doublet ground state, δ, to be <1.0 cm^{-1}. D and J values in eq 2 that give a δ value between 0.2 and 1.0 cm^{-1} are also given in Figure 9A (— and - - -). Figure 9A presents a solution space for the component of the two-azide-bound R2 complex having $g_{||} = 16$ in terms of J and D. The region shown in Figure 9A is consistent with the qualitative discussion of the saturation−magnetization data: $J > 0$ corresponding to ferromagnetic coupling and $D_{1,2} < 0$ corresponding to the (4, ± 4) ground state.

From Figure 9A the magnitudes of J and D are constrained to a limited region in solution space in order to fit both the first excited state and the zero-field splitting data. J values range from 1.0 to 8.0 cm^{-1}, while $D_1 = D_2$ are constrained to lie between -6 and -16 cm^{-1}. From the VTVH MCD data, $g_{||}$ is determined to be 16.0 ± 0.5. Figure 9B presents the $g_{||}$ values obtained over a range of J and D values. Values of $g_{||} \sim 16$ are obtained if $0.5 < J < 1.5$ cm^{-1} and the entire range of D are possible solutions. Taking into account the location of the (4,

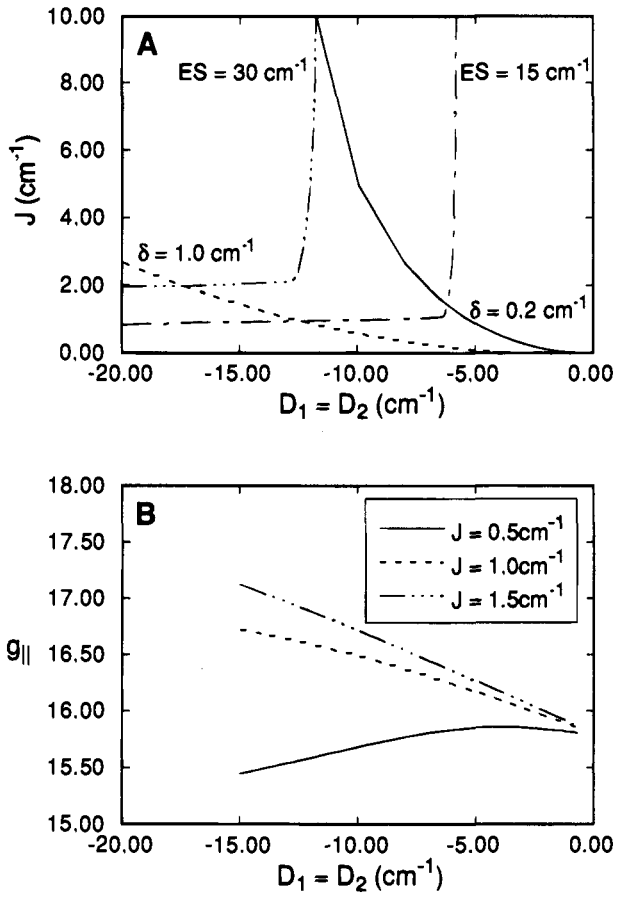

Figure 9. D vs J solution space for the ferromagnetically coupled two-azide-bound R2 complex in terms of δ, $g_{||}$, and the energy of the first excited state (ES). (A) presents curves showing the values of D and J which produce energy levels such that the first excited state doublet is between 15 and 30 cm^{-1}. The axial ZFS parameters for the two iron atoms are constrained to be equal. (B) shows the $g_{||}$ values obtained over a range of J and $D_1 = D_2$ values for the two-azide-bound complex.

0; 3, 0) doublet as the first excited state at ~15.0 cm^{-1} limits J to approximately 1.0 cm^{-1}. Allowing the D values to become unequal does not further restrict the solution space. The results from the spin Hamiltonian analysis for the $g_{||}$ ~16 component of the two-azide-bound form are given in Table 3.

In summary, binding a second azide to the one-azide-bound form of reduced R2 produces two distinguishable binuclear ferrous components. One species consists of one four- and one six-coordinate Fe(II) site where the ferrous atoms are weakly coupled ($-2.0 < J < 2.0$ cm^{-1}) and have unequal D values consistent with iron atoms in different environments. The D values must have opposite sign in order to accommodate the $g_{||}$ ~8, $M_S = \pm 2$ doublet ground state. In contrast, the second component of the two-azide-bound form has one five- and one six-coordinate Fe(II) atom. The spin Hamiltonian analysis confirms that this component is weakly ferromagnetically coupled and therefore requires $J > 0$ cm^{-1} and $D_{1,2} < 0$ cm^{-1}. This indicates that upon azide binding to this site the positive D value has changed sign, consistent with the four-coordinate Fe(II) center becoming five-coordinate.

Discussion

A reasonable working model of the fully reduced R2 active site based on the spectroscopic results presented in this study is shown in Scheme 2. The CD and MCD data analyzed above indicate that the active site of the reduced R2 subunit of RDPR has one four-coordinate and one five-coordinate ferrous center. The magnetic data show that the native ferrous protein has a $M_S = \pm 2$ ground state, due to the iron ions being antiferromagnetically coupled with $J \approx -0.5$ cm^{-1} and the D values being of opposite signs. The structure of the reduced R2 active site indicated by CD and MCD can be correlated to the crystal structure of the manganese-substituted R2.[52] The crystal structure shows one four- and one five-coordinate Mn(II) atom which are bridged by two carboxylate residues. The magnitude of the observed exchange coupling in fully reduced R2 is consistent with the presence of two μ-1,3-carboxylate bridges.[62,63] While preliminary crystallographic data on the reduced iron site structure of RDPR suggest that the active site consists of two four-coordinate Fe(II) atoms,[35] this is not consistent with the presence of three ligand field transitions in the 5000 to 10000 cm^{-1} region.

Azide binds to reduced R2 with two binding constants. The first azide appears to bind to an open coordination position on the five-coordinate iron in reduced R2, resulting in hexacoordination. In addition the magnetic properties of the protein are affected by azide binding, indicating a new ground state. The one-azide-bound complex shows behavior consistent with a $M_S = \pm 1$ ground state, which requires an increase in antiferromagnetic coupling between the two Fe(II) atoms in the active site (see Figure 6C). Since the modification in antiferromagnetic exchange upon binding the first azide is relatively small, it is likely that the bridging pathway is not significantly perturbed upon formation of the one-azide-bound complex, suggesting that the azide does not bridge which is consistent with one Fe(II) atom remaining four-coordinate.

Addition of the second azide results in more significant changes of the active site structure. The second azide appears to coordinate to the open coordination position on the four-coordinate Fe(II) in the one-azide-bound complex, resulting in the formation of two distinct two-azide-bound binuclear ferrous complexes. One [Fe(II)Fe(II)] cluster has one five- and one six-coordinate ferrous site. In addition a large change is seen in the magnetic properties of the protein, indicating a new ground state. This azide complex shows behavior consistent with a $M_S = \pm 4$ ground state, which requires ferromagnetic exchange coupling.

Two ferromagnetically coupled ferrous centers have also been observed in deoxy-azide Hr[36,58] and in the fully reduced hydroxylase component of MMO.[37,64] The ferromagnetic coupling in deoxy-azide Hr is proposed to arise from the presence of a H_2O bridge in the biferrous active site. By analogy, the $g_{||}$ ~17 EPR signal observed for reduced R2 with azide has been interpreted in terms of a water bridge.[34] However, the presence of a water bridge in the two-azide-bound R2 complex may be less likely for a number of reasons. First, in the case of deoxy-azide Hr the water bridge would result from protonation of the hydroxide bridge present in deoxyHr.[36] However, reduced R2 has only carboxylate bridging ligands. Second, although the crystal structure of the Mn(II)-reconstituted R2[52] indicates the presence of a coordinated water that may be converted into a μ-aquo bridge, formation of such a bridge would require a large rearrangement of the ligands coordinated to the RDPR active site in order to accommodate the Fe(II) geometries indicated by CD and MCD. Third, in Hr the hydroxo bridge which can be further protonated to form a H_2O bridge appears to be endogenous and not derived from exog-

(62) Tolman, W. B.; Liu, S.; Bentsen, J. G.; Lippard, S. J. *J. Am. Chem. Soc.* **1991**, *113*, 152.
(63) Cheng, C.; Reiff, W. M. *Inorg. Chem.* **1977**, *16*, 2097.
(64) Hendrich, M. P.; Münck, E.; Fox, B. G.; Lipscomb, J. D. *J. Am. Chem. Soc.* **1990**, *112*, 5861.

Scheme 2

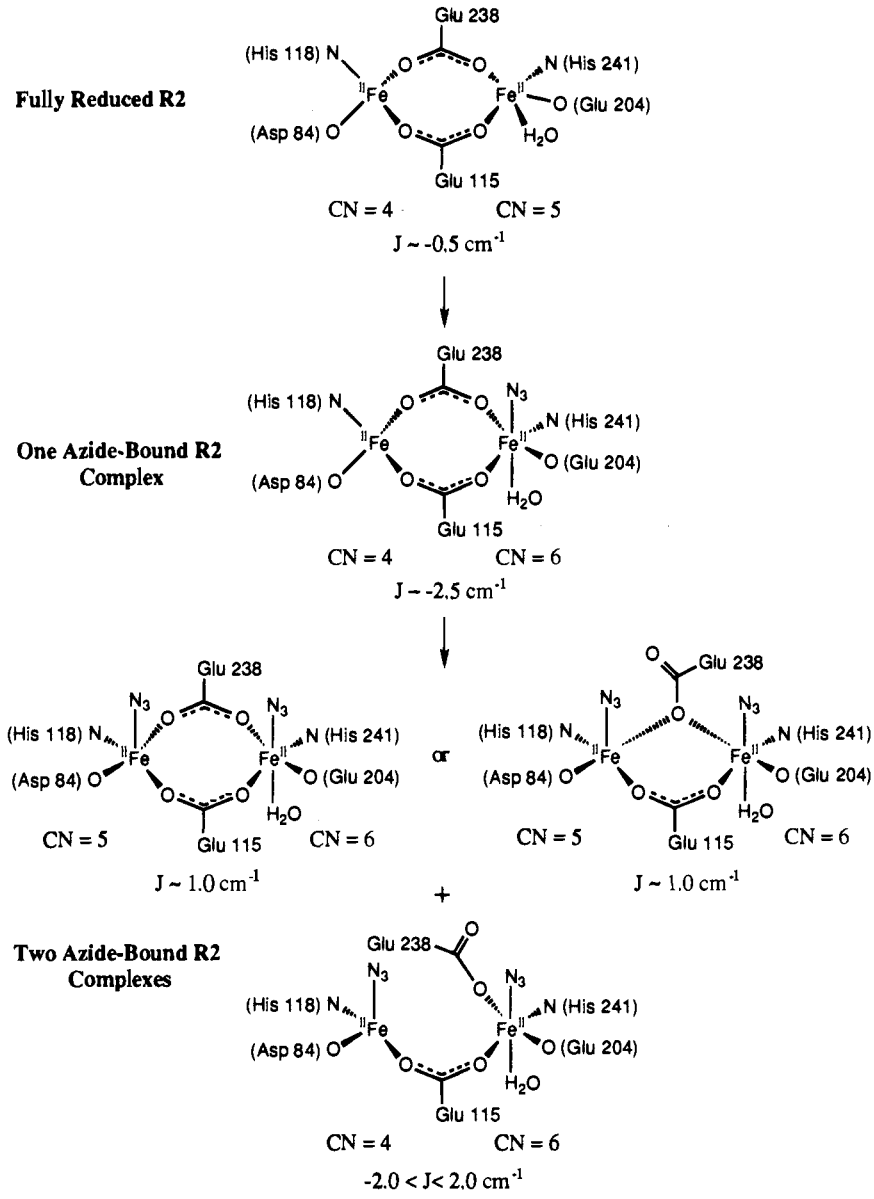

enous O_2 and may play a role in H^+ donation to O_2.[36] Alternatively, for RDPR the exogenous O_2 produces the μ-oxo bridge.[30]

For the reduced hydroxylase component of MMO, a H_2O bridge was initially suggested for the active site to account for the observed ferromagnetic coupling.[37] Crystallographic data, however, indicate that the binuclear ferrous center of reduced hydroxylase is bridged by two carboxylate ligands: one in a μ-1,3 and the other in a μ-1,1 bridging mode.[39] It is possible that the latter bridge is primarily responsible for the ferromagnetic exchange coupling.[62] Crystallographic data have shown that reduced R2 has two μ-1,3-carboxylate bridging ligands[35,52] which mediate weak antiferromagnetic coupling (*vide supra*). A possible explanation for the observed ferromagnetic coupling in one component of the two-azide-bound form of R2 would be the occurrence of a carboxylate shift[65] such that one carboxylate ligand is reoriented from a μ-1,3 to a μ-1,1 bridging mode. Alternatively, if the carboxylate ligand remains in a μ-1,3 bridging mode, ligation of the second azide could simply change the effectiveness of the exchange pathways by perturbing the orientation of the orbital containing the extra electron, possibly inducing the observed ferromagnetic coupling (Scheme 2).

The second component of the two-azide-bound form consists of one four-coordinate and one six-coordinate ferrous iron. The magnetic data indicate that the ground state of this complex is a $M_s = \pm 2$ doublet requiring the ZFS D values of the iron atoms to be of opposite signs. These results are consistent with both weak antiferro- or weak ferromagnetic exchange coupling. It should also be reemphasized that despite having similar Fe(II) coordination environments this two azide-bound form is not simply unconverted one-azide-bound complex since its ground state is a $M_s = \pm 2$ doublet not the ± 1 doublet of the one-azide-bound species. A possible explanation for the presence of a four-coordinate Fe(II) atom is that the azide competes with the bridging carboxylate ligand at the four-coordinate Fe(II), thereby altering the binding mode of the carboxylate from bridging bidentate to terminal monodentate. A similar displacement is observed upon oxidation of the reduced R2 site where the bridging carboxylate is replaced by the oxo bridge.[5] Since increasing the concentration of azide does not change the product distribution of the two two-azide-bound complexes, these are two distinct products. Thus, as summarized at the bottom of

(65) Rardin, R. L.; Tolman, W. B.; Lippard, S. J. *New J. Chem.* **1991**, *15*, 417.

Scheme 2, the difference in properties between the two different two-azide-bound components could arise from partial loss of a bridging carboxylate ligand from one of the Fe(II) ions which would result in a change in coordination number.

The results of the ligand titration studies presented above indicate that there is an open coordination position on each Fe(II) atom in the reduced R2 active site leading to the possibility of dioxygen bridging between the two iron atoms.[49] Resonance Raman studies have shown that the μ-oxo bridge present in oxidized R2 originates from molecular oxygen,[30] supporting the possible formation of a μ-1,1-hydroperoxide intermediate.[49] The azide binding studies presented above directly address the question of small molecules bridging the binuclear iron site. Azide, like dioxygen, can bind to a binuclear metal center in a number of ways, as a terminal ligand or in a μ-1,1 or μ-1,3 bridging mode. The results of the current study indicate that azide does not bridge the binuclear ferrous site of R2. It is possible that the ferrous active site has a higher affinity for the endogenous carboxylate bridge and that one azide cannot compete effectively with this bridge.

In summary, the spectroscopic protocol applied in this study has provided important insight into the binuclear iron active site of the fully reduced R2 subunit of RDPR. The coordination geometry of the ferrous site in reduced R2, the one-azide-bound R2 complex, and the two-azide-bound R2 complex has been determined. CD and MCD studies have shown that the binuclear ferrous active site of the R2 subunit of RDPR consists of one four- and one five-coordinate Fe(II) atom that are weakly antiferromagnetically coupled. Azide binding studies reveal that reduced R2 binds two molecules of azide with distinct binding constants. The spectroscopic results presented above suggest that binding of the first azide converts the five-coordinate Fe(II) atom of reduced R2 into a six-coordinate species, but otherwise does not dramatically perturb the active site. In contrast, binding the second has a more profound effect. The two-azide-bound form exists as a mixture of species. One component is ferromagnetically coupled and most likely has one five- and one six-coordinate Fe(II) center. The other component is antiferromagnetically coupled and is four- plus six-coordinate leading to the possibility that the second azide competes with an endogenous carboxylate bridge. Finally, these studies suggest that both Fe(II) atoms have an open coordination position, such that an exogenous ligand (i.e., O_2) may react with both iron atoms of the reduced site in a bridging fashion.

Acknowledgment. This work was supported by the NSF-Biophysics Program Grant MCB 9316768 (E.I.S.) and NIH GM29595 (J.S.). We thank Dr. Cecelia Campochiaro for many helpful discussions during the course of this study and for writing the computer programs used to fit the magnetic susceptibility data.

JA952905W